Paleoceanography and Paleoclimatology

AGU ADVANCING EARTH AND SPACE SCIENCE

RESEARCH ARTICLE
10.1029/2022PA004529

Special Section:
DeepMIP in the Hothouse Earth: late Paleocene-early Eocene climates and their lessons for the future

Revisiting the Geographical Extent of Exceptional Warmth in the Early Paleogene Southern Ocean

J. Frieling[1,2], S. M. Bohaty[3], M. J. Cramwinckel[1], S. J. Gallagher[4], G. R. Holdgate[5], T. Reichgelt[6], F. Peterse[1], J. Pross[3], A. Sluijs[1], and P. K. Bijl[1]

[1]Department of Earth Sciences, Faculty of Geosciences, Utrecht University, Utrecht, The Netherlands, [2]Now at Department of Earth Sciences, University of Oxford, Oxford, UK, [3]Institute of Earth Sciences, Heidelberg University, Heidelberg, Germany, [4]School of Geography, Earth and Atmospheric Sciences, The University of Melbourne, Melbourne, VIC, Australia, [5]Geotrack International, Brunswick West, VIC, Australia, [6]Department of Geosciences, University of Connecticut, Storrs, CT, USA

Abstract To assess zonal temperature and biogeographical patterns in the Southern Ocean during the Paleogene, we present new multi-proxy air- and sea-surface temperature data for the latest Paleocene (~57–56 Ma) and the Paleocene-Eocene Thermal Maximum (PETM; ~56 Ma) from the northern margin of the Australo-Antarctic Gulf (AAG). The various proxy data sets document the well-known late Paleocene warming and, superimposed, two transient late Paleocene pre-cursor warming events, hundreds of kyr prior to the PETM. Remarkably, temperature reconstructions for the AAG and southwest Pacific during the latest Paleocene, PETM and Early Eocene Climatic Optimum (~53–49 Ma) show similar trends as well as similar absolute temperatures east and west of the closed Tasmanian Gateway. Our data imply that the exceptional warmth as recorded by previous studies for the southwest Pacific extended westward into the AAG. This contrasts with modeling-derived circulation and temperature patterns. We suggest that simulations of ocean circulation underestimate heat transport in the southwest Pacific due to insufficient resolution, not allowing for mesoscale eddy-related heat transport. We argue for a systematic approach to tackle model and proxy biases that may occur in marginal marine settings and non-analog high-latitude climates to assess the temperature reconstructions.

Plain Language Summary For the Cenozoic (past 66 million years) there is a good correspondence between climate conditions derived from numerical models and those from reconstructions on sediment cores, but in some regions fundamental discrepancies between the two require further understanding. We test the extent and potential origin of a remaining discrepancy: the Paleocene-Eocene southwest Pacific. In this region proxy-based sea surface temperature reconstructions are much warmer than modeled. Our new temperature reconstructions from the Australo-Antarctic Gulf are strikingly similar to those from the southwest Pacific, while the closed Tasmanian Gateway separates these two basins into fundamentally different oceanographic settings. The overall pattern might be attributed to systematic underestimation of high-latitude warm-current invasion in low-resolution climate models. A better understanding of temperature proxies in non-analog climates is likely also required to validate the exceptional high-latitude warmth recorded in our data.

Key Points:

- Temperature reconstructions for the late Paleocene and Paleocene-Eocene Thermal Maximum show identical temperature in the Australo-Antarctic Gulf and the SW Pacific
- The zonally identical temperatures contrast with climate model runs and projected ocean currents
- The relatively low spatial resolution of current climate models may underestimate heat transport from meso-scale eddies to the SW Pacific

Supporting Information:

Supporting Information may be found in the online version of this article.

Correspondence to:

J. Frieling and P. K. Bijl,
joost.frieling@earth.ox.ac.uk;
p.k.bijl@uu.nl

Citation:

Frieling, J., Bohaty, S. M., Cramwinckel, M. J., Gallagher, S. J., Holdgate, G. R., Reichgelt, T., et al. (2023). Revisiting the geographical extent of exceptional warmth in the Early Paleogene Southern Ocean. *Paleoceanography and Paleoclimatology*, *38*, e2022PA004529. https://doi.org/10.1029/2022PA004529

Received 15 AUG 2022
Accepted 10 FEB 2023

Author Contributions:

Conceptualization: J. Frieling, S. M. Bohaty, S. J. Gallagher, J. Pross, P. K. Bijl
Formal analysis: J. Frieling, M. J. Cramwinckel, T. Reichgelt, F. Peterse
Funding acquisition: P. K. Bijl

1. Introduction

Periods of transient warming superimposed on sustained greenhouse climates during the Paleocene and Eocene (early Paleogene; ca. 66–34 Million years ago (Ma)) may be employed as potential analogs for current climate change and potential end-member climate states under unabated carbon emissions (Burke et al., 2018). A negative carbon isotope excursion (CIE), globally recorded in terrestrial and marine sediments, combined with ocean acidification (McInerney & Wing, 2011; Zachos et al., 2005) at the onset of the Paleocene-Eocene Thermal Maximum (PETM; 56 Ma) shows the rapid input of thousands of petagrams of ^{13}C-depleted C to the exogenic carbon pool (Dickens et al., 1995), providing a geologic analog to present-day anthropogenic emissions. Several smaller events appear to have occurred in the late Paleocene and throughout the early Eocene (Cramer et al., 2003; Lauretano et al., 2015; Westerhold et al., 2020) although their climatic expression remains unknown.

In recent years, fully coupled climate models have been able to broadly reproduce sea-surface and air temperature proxy data for the warmest periods of the Cenozoic (Cramwinckel et al., 2018; Evans et al., 2018; Lunt et al., 2021). Similarly, the models can reproduce the magnitude of extreme transient warming across the PETM

Investigation: J. Frieling, S. M. Bohaty, M. J. Cramwinckel, T. Reichgelt, F. Peterse, J. Pross, A. Sluijs, P. K. Bijl
Methodology: J. Frieling
Resources: S. J. Gallagher, G. R. Holdgate, P. K. Bijl
Supervision: P. K. Bijl
Visualization: J. Frieling
Writing – original draft: J. Frieling
Writing – review & editing: S. M. Bohaty, M. J. Cramwinckel, S. J. Gallagher, G. R. Holdgate, T. Reichgelt, F. Peterse, J. Pross, A. Sluijs, P. K. Bijl

(Dunkley Jones et al., 2013; Frieling et al., 2017; Hollis et al., 2019; Lunt et al., 2021; Zhu et al., 2019). This suggests that such models provide accurate reflections of global climate states and meridional gradient changes under high radiative forcing. However, even in simulations where the majority of the reconstructed sea-surface temperature (SST) patterns and deep-ocean temperatures are consistent with model output throughout the Eocene, absolute temperature reconstructions from several regions, notably the Arctic and the southwest (SW) Pacific Ocean, and in particular the area around the Tasmanian Gateway (TG) and Zealandia, are still much (>10°C) warmer than those in the simulations (Cramwinckel et al., 2018; Evans et al., 2018; Frieling et al., 2017; Lunt et al., 2021). In contrast to the reconstructions showing exceptional regional warmth, the Southern Ocean, including the south Pacific Ocean, was likely the dominant locus of cold deep-water formation during much of the Paleogene (Huck et al., 2017; Pak & Miller, 1992), highlighting the importance of resolving the paleoceanography and mechanistic understanding of the enigmatic warmth in and around the SW Pacific (Bijl et al., 2009; Douglas et al., 2014; Hollis et al., 2009).

During the PETM and early Eocene climate optimum (EECO; ~53–49 Ma), SST estimates from the SW Pacific and the Antarctic margin of the Australo-Antarctic Gulf (AAG) (Figure 1) both consistently exceed 30°C, and megathermal vegetation elements were established (Bijl, Bendle, et al., 2013; Bijl et al., 2009, 2021; Carpenter et al., 2012; Contreras et al., 2013, 2014; Hollis et al., 2015; Huurdeman et al., 2021; Pross et al., 2012; Reichgelt et al., 2022; Sluijs et al., 2011). Moreover, dinoflagellate cyst (dinocyst) biogeography suggests that the surface circulation was dominated by low and high latitude-derived currents in the AAG and SW Pacific (Figure 1a), respectively (Bijl, Sluijs, et al., 2013; Bijl et al., 2011). These interpretations are broadly supported by modeling efforts (Huber et al., 2004) and such a regional circulation pattern results in consistently higher modeled SST in the northern AAG compared to the SW Pacific (e.g., Hollis et al., 2009, Figure 1b). It is noteworthy that although proxy-derived SSTs for the SW Pacific are >10°C higher than the model-derived SSTs (e.g., Lunt et al., 2021) during the Early Eocene Climatic Optimum (EECO), mean annual air temperature (MAAT) reconstructions can be matched by current models (Lunt et al., 2021; Reichgelt et al., 2022).

Regional paleoceanography, especially the gradual opening of the TG, would have affected regional temperature trends through re-routing of warm versus cold ocean currents (Bijl, Bendle, et al., 2013; Bijl, Sluijs, et al., 2013; Cande & Stock, 2004; Sijp et al., 2014, 2016). Recent efforts to constrain the consequence of gradual gateway opening suggest that the regional climatic impact of both the Drake Passage and TG is limited, unless both allow relatively deep throughflow simultaneously (Sauermilch et al., 2021), a situation that does not seem to have occurred until ca. 26 Ma (van de Lagemaat et al., 2021). Therefore, even if a shallow (<300 m water depth) connection existed during the Paleocene and early Eocene (Bijl, Bendle, et al., 2013; Sauermilch et al., 2021), it should have had a negligible impact on paleoceanography and heat transport. On the other hand, in very high-resolution model simulations (<1°), warm mesoscale eddies reach further south than any current in low-resolution runs. Therefore, substantial differences in modeled surface-water temperatures in parts of the SW Pacific arise between the low-resolution and eddy-permitting model runs. Such oceanographic features can presumably reduce the temperature difference between the SW Pacific and the AAG directly surrounding the TG (Nooteboom et al., 2022).

Unfortunately, however, no well-dated temperature proxy or biogeographical data from the northern margin of the AAG, presumably the warmest place in this region, are available for some key intervals of the Paleogene, notably the latest Paleocene (ca. 57–56 Ma) and the PETM. These periods, along with the EECO, deserve particular attention as they are targeted by community data-model comparison efforts such as DeepMIP (Hollis et al., 2019; Lunt et al., 2017, 2021). However, the absence of data hampers the comparison of temperatures on both sides of the TG, the reconstruction of regional oceanography, and the establishment of a regional temperature response pattern. Consequently, in-depth assessment of model performance is limited, which is crucial in light of the apparent proxy-model mismatch.

To fill this data gap, we present new multi-proxy SST and MAAT estimates for two expanded late Paleocene-PETM sedimentary successions from the AAG, deposited in shallow-marine settings at ~60°S paleolatitude (Otway Basin (OB), Victoria, Australia, Figure 1) (Frieling et al., 2018; Huurdeman et al., 2021). To reconstruct temperature, we applied a suite of lipid biomarker proxies (Table 1) and palynological tools. We supplement the MAAT reconstructions of the latest Paleocene based on nearest-living relative (NLR) analyses of sporomorph assemblages and branched glycerol dialkyl glycerol tetraethers (brGDGTs) (Huurdeman et al., 2021). In addition, we analyze novel proxies proposed to reflect paleotemperature based on branched glycerol monoalkyl glycerol

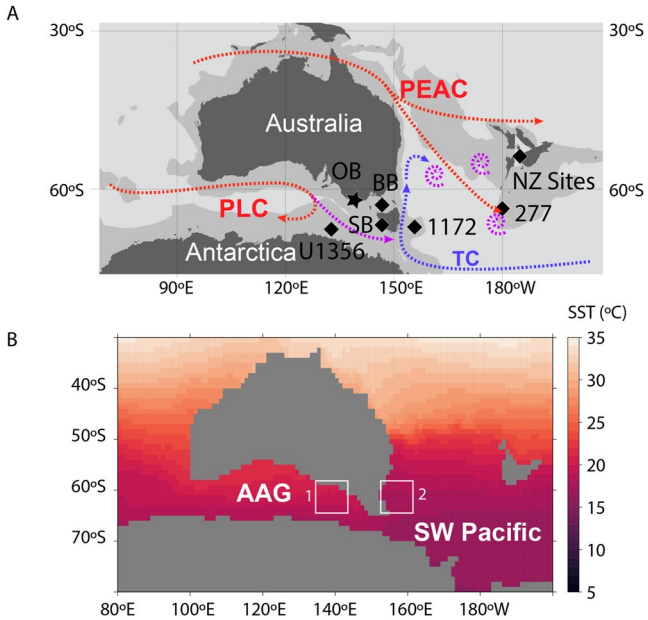

Figure 1. Paleogeographical reconstruction of the Tasmanian Gateway area around 56 Ma (Müller et al., 2019). (a) Location of Point Margaret and Latrobe-1 (star) and previously used sites (diamonds) for which data was generated and compiled, respectively. Abbreviations: OB, Otway Basin: Point Margaret and Latrobe-1; BB, Bass Basin (Konkon-1, Poonboon-1); SB, Sorrell Basin (Lowana Road), Tasmania, U1356 = Integrated Ocean Drilling Program Site U1356, 1172 = Ocean Drilling Program Site 1172, 277 = Deep Sea Drilling Project Site 277, NZ Sites = multiple sites in New Zealand (Mid-Waipara, Tora, Tawanui, Otaio River). For modern locations see Figure S1 in Supporting Information S1. Other abbreviations: PLC, Proto-Leeuwin Current; TC,Tasman Current; PEAC, Proto East Australia Current. Biogeography and simplified model-based currents; red, purple and blue arrows indicate low-latitude, transitional and Antarctic-derived surface currents and eddies, respectively (Bijl, Bendle, et al., 2013; Nooteboom et al., 2022; Sauermilch et al., 2019). (b) Regional modeled sea-surface temperature (SST). Model run represents a high pCO_2 (6x pre-industrial pCO_2) of CESM1.2 (Lunt et al., 2021; Zhu et al., 2019). Note higher SST in the Australo-Antarctic Gulf (box 1) compared to the southwest (SW) Pacific (box 2) at the same latitude.

tetraethers (brGMGTs) (Baxter et al., 2019; Naafs, McCormick, et al., 2018) and the relative abundance of isoprenoid glycerol dialkyl glycerol tetraethers (isoGDGTs) with five cyclopentane moieties (%GDGT-5) (Naafs, Rohrssen, et al., 2018). Furthermore, we applied the TetraEther index of tetraethers consisting of 86 carbon atoms (TEX_{86}) paleothermometer to estimate sea (sub-)surface temperature (Kim et al., 2010; Schouten et al., 2002) and support this record by assessing the relative abundances of crenarchaeol-isomer to total crenarchaeol (f(cren')) that depends on temperature in culture studies (Bale et al., 2019; O'Brien et al., 2017; Sinninghe Damsté et al., 2012). Dinocysts produced by thermophilic dinoflagellates and mangrove palm pollen were used to acquire minimum temperature thresholds. Temperature estimates for the AAG are paired with previously published data from the SW Pacific to assess temperature differences across the TG.

2. Materials and Methods

2.1. Materials and Setting

Samples from the Latrobe-1 core (38° 41′ 35″S, 143° 09′ 00″E) and the Point Margaret outcrop (~3 km east; 38° 43′ 28.8″S, 143° 10′ 35″E) near Port Campbell, Victoria, Australia were analyzed. A description of sample collection, lithology and stratigraphy of the section was given by Frieling et al. (2018). Point Margaret, a coastal cliff outcrop section, is composed of shallow-marine deposits marked by a gradual up-section transition from (pro-)deltaic muddy sandstones to sandy silt and mudstones, with 0.5%–3% organic matter (Figure 2, Figure S9 in Supporting Information S1). Combined bio- and carbon isotope stratigraphy suggest that the upper ~35 m of the Point Margaret section cover at most ~500 kyr of the latest Paleocene (56.5–56 Ma), and the base of the Paleocene section is deemed younger than ca. 57 Ma (Frieling et al., 2018). The top of the outcrop is covered by modern soils truncating the "body" of the CIE of the PETM, as suggested by carbon isotope stratigraphy.

The Latrobe-1 core, although in some intervals marked by sparse recovery, shows a similar lithology dominated by sandy-siltstones as the Point Margaret outcrop. The Latrobe-1 core extends into the EECO based on dinocyst and sporomorph biostratigraphy (Frieling et al., 2018). Sediments were deposited in a subsiding trough system, allowing for rapid and almost continuous sediment accumulation during continental rifting (Sauermilch et al., 2019). In contrast to offshore deposits of the same age, the onshore successions analyzed here were not positioned in the depocenter of the OB and were never deeply buried by later Paleogene or Neogene material (Arditto, 1995). Indeed, organic microfossils suffered minimal oxic degradation or even compression and show no signs of thermal alteration. Since the Latrobe-1 core recovery is sub-optimal in sandy strata and in critical intervals, and since the material has degraded during core storage (Frieling et al., 2018), we refrain from constructing a composite or spliced section with the Point Margaret succession.

The regional oceanography of the SW Pacific in the early Paleogene is thought to have been characterized by the Antarctica-derived Tasman Current (TC) in the southernmost sector (Figure 1a, Bijl et al., 2011; Huber et al., 2004; Sauermilch et al., 2019, and references therein). Further north, the influence of the lower-latitude Proto-East Australia Current becomes pronounced. The low latitude Proto-Leeuwin Current entered the AAG in the west and extended progressively further east as the AAG widened during the Cenozoic.

We here focused on the latest Paleocene and PETM (Frieling et al., 2018) in both sections.

2.2. Methods—Palynology

Detailed dinocyst assemblage data were generated for 94 samples from Point Margaret and 20 samples from the Latrobe-1 core. A minimum of 200 and 300 specimens were determined to the species level for dinocysts and

Paleoceanography and Paleoclimatology

10.1029/2022PA004529

Table 1
Lipid Compounds and Proxies

Lipid group	Compounds	Mass fragment chromatograms (*m/z*)
Isoprenoid GDGTs	isoGDGT-0, 1, 2, 3, 5	1302, 1300, 1298, 1296, 1292
Crenarchaeol	Crenarchaeol and crenarchaeol stereoisomer (cren')	1292
Branched GDGTs	IIIa, IIIa', IIIb, IIIb', IIIc, IIIc', IIa, IIa', IIb, IIb', IIc, IIc', Ia, Ib, Ic	1050, 1048, 1046, 1036, 1034, 1032, 1022, 1020, 1018
Branched GMGTs	H1048, H1034a, H1020a, H1020b, H1020c	1048, 1034, 1020

Proxy	Main use	Based on:	Original/key reference	Calibration error/ cut-off value
TEX_{86}	Sea surface temperature	isoGDGT-2 + isoGDGT-3 + cren'/isoGDGT-1 + isoGDGT-2 + isoGDGT-3 + cren'	Kim et al. (2010), O'Brien et al. (2017), and Schouten et al. (2002)	2.5°C (TEX_{86}^{H})
Methane Index (MI)	Impact of methanogens/ methanotroph-derived isoGDGTs on TEX_{86}	isoGDGT-1 + isoGDGT-2 + isoGDGT-3/ isoGDGT-1 + isoGDGT-2 + isoGDGT-3 + cren' + crenarchaeol	Zhang et al. (2011)	0.3
Methane Index (MI)	Impact of methanotroph-derived isoGDGTs on TEX_{86}	isoGDGT-2/crenarchaeol	Weijers et al. (2011)	0.2
Ring Index (RI)	Impact of non-thermal isoGDGT production on TEX_{86}	0 × isoGDGT-0 + 1 × isoGDGT-1 + 2 × isoGDGT-2 + 3 × isoGDGT-3 + 4 × cren' + 4 × crenarchaeol	Zhang et al. (2016)	|0.3| ΔRI
[2/3]	Deep-water-derived isoGDGT impact on TEX_{86}	isoGDGT-2/isoGDGT-3	Hurley et al. (2018) and Taylor et al. (2013)	5
f(cren')	Temperature trends*, non-thermal behavior in TEX_{86}	cren'/cren' + crenarchaeol	Bale et al. (2019), O'Brien et al. (2017), and Sinninghe Damsté et al. (2012)	0.003 (analytical reproducibility)
MBT'_{5Me}	Soil temperature	Ia + Ib + Ic/Ia + Ib + Ic + IIa + IIb + IIc + IIIa	De Jonge, Hopmans, et al. (2014)	4.8°C
$MBT_{acyclic}$	Soil temperature	Ia/Ia + IIa + IIIa	Weijers et al. (2007)	–
CBT'_{5Me}	Soil pH	−log Ib + IIb/Ia + IIa	De Jonge, Hopmans, et al. (2014)	–
BIT	Relative amount of soil organic matter in marine sediment	IIIa + IIIa' + IIa + IIa' + Ia/crenarcheaol + IIIa + IIIa' + IIa + IIa' + Ia	Hopmans et al. (2004) and Weijers et al. (2006)	0.3/location dependent

Proxy	Main use	Based on:	Original/key reference	Calibration error/ cut-off value
Isomer ratio (IR)—methylated compounds	Non-soil production of brGDGTs	IIa' + IIb' + IIc' + IIIa' + IIIb' + IIIc'/ IIa + IIa' + IIb + IIb' + IIc + IIc' + IIIa + IIIa' + IIIb + IIIb' + IIIc + IIIc'	De Jonge, Stadnitskaia, et al. (2014) and Sinninghe Damsté (2016)	Soil dependent
brGMGTI	Lake water temperature*	H1020c + H1034a + H1034c/H1020b + H1020c + H1034a + H1034b + H1034c + H1048	Baxter et al. (2019)	2.2°C
$HMBT_{acyclic}$	Temperature*	H1020c/H1020c + H1034b + H1048	Bijl et al. (2021), Naafs, McCormick, et al. (2018), and Sluijs et al. (2020)	–
%brGMGT	Temperature*	sum(brGMGTs)/(sum(brGMGTs) + sum(brGDGTs))	Naafs, McCormick, et al. (2018)	–
%iGDGT-5	Soil temperature threshold (19°C)*	isoGDGT-5/isoGDGT-1 + isoGDGT-2 + isoGDGT-3 + isoGDGT-5	Naafs, Rohrssen, et al. (2018)	–

Note. Note that the Ring Index is based on fractional abundance of isoGDGTs and that the difference with TEX_{86}-derived Ring Index ($RI_{TEX} = -0.77 \times TEX_{86} + 3.32 \times TEX_{86}^2 + 1.59$) is calculated to obtain ΔRI. *indicates Proxies here tested outside their originally Proposed use or environment of origin.

terrestrial palynomorphs, respectively, in the palynological samples used for biostratigraphy by Frieling et al. (2018). Dinocyst taxonomy follows G. L. Williams et al. (2017) except for the subfamily Wetzelielloideae, where we follow Bijl et al. (2016). We refer to Huurdeman et al. (2021) for details on the pollen and spore taxonomy.

Pollen and spore assemblages of seven samples from the Latrobe-1 core and 61 from Point Margaret were used to generate temperature reconstructions based on probabilistic climate envelopes of NLR distributions (e.g., Huurdeman et al., 2021; Willard et al., 2019). The occurrence and abundance of particularly temperature-sensitive dinocyst taxa, including *Apectodinium* spp. (>20°C) and *Florentinia reichartii* (>25°C) (Frieling & Sluijs, 2018) were used as thresholds to quantify minimum SST. Additionally, the presence of mangrove palm *Nypa* pollen (Huurdeman et al., 2021; Reichgelt et al., 2018) was used to provide complementary thresholds on minimum MAAT. Abundance counts for *Nypa* pollen were generated for the top part of the succession at Point Margaret (47–52.3 m). Samples below 47 m at Point Margaret and early Eocene samples in the Latrobe-1 were only scanned for the absence versus presence of *Nypa*.

2.3. Methods—Organic Geochemistry

A total of 114 samples was analyzed for branched and isoprenoid GDGTs and brGMGTs; 94 for Point Margaret and 20 for the Latrobe-1 core. 54 of the samples from Point Margaret had already been extracted and analyzed for brGDGTs by Huurdeman et al. (2021), and resulting chromatograms were used for identification and quantification of isoGDGTs and brGMGTs here. The remaining samples were prepared following the same procedure as used by Huurdeman et al. (2021). In short, 10–15 g of freeze-dried sediment was extracted using an accelerated solvent extractor using 9:1 (volume:volume) dichloromethane:methanol and subsequently separated into apolar and polar fractions over activated aluminum oxide. The polar fractions, containing the GDGTs and GMGTs were dissolved in 99:1 hexane:isopropanol, filtered over a 0.45 μm polytetrafluoroethylene filter, and measured on an Agilent 1260 ultra-high performance liquid chromatograph—mass spectrometer (UHPLC-MS) with settings according to Hopmans et al. (2016). GDGTs and GMGTs were identified by detecting the [M+H]+ ions in selected ion monitoring mode at *m/z* 1302, 1300, 1298, 1296, 1292, 1050, 1048, 1046, 1036, 1034, 1032, 1022, 1020, 1018, and using *m/z* 744 for the internal standard (a synthetic C_{46}). A minimum peak area cut-off (3,000 units) was applied for individual components, which here typically amounts to absolute concentrations below 1 ng g^{-1} dry sediment or ~10 μg g^{-1} total organic carbon (TOC).

2.4. Methods—Organic Geochemical Proxies

2.4.1. MBT'_{5me} and CBT'_{5me}

The methylation and cyclization of brGDGTs, quantified in the Methylated of Branched Tetraethers (MBT'_{5Me}) and Cyclisation of Branched Tetraethers (CBT'_{5Me}), respectively, was originally linked to soil temperature and pH (Weijers et al., 2007). Subsequent improvements to the liquid chromatograph-mass spectrometer (LC-MS) methodology resulted in identification and clearer separation of brGDGT isomers with a methylation on the fifth or the sixth position (indicated with an '), which allowed disentangling these two environmental controls on brGDGT distributions (De Jonge, Hopmans, et al., 2014). Here, we apply the MBT'_{5Me} based on the methylation of 5-methyl brGDGTs to extend the existing late Paleocene and PETM MAAT reconstruction (Huurdeman et al., 2021) to the base of the Point Margaret section. To verify soils as primary source of the brGDGTs in these sections, brGDGT distributions are compared to modern global soil and peat data sets (Figure S11 in Supporting Information S1) (De Jonge, Hopmans, et al., 2014; Hollis et al., 2019; Huurdeman et al., 2021; Naafs, Gallego-Sala et al., 2017; Naafs, Inglis,

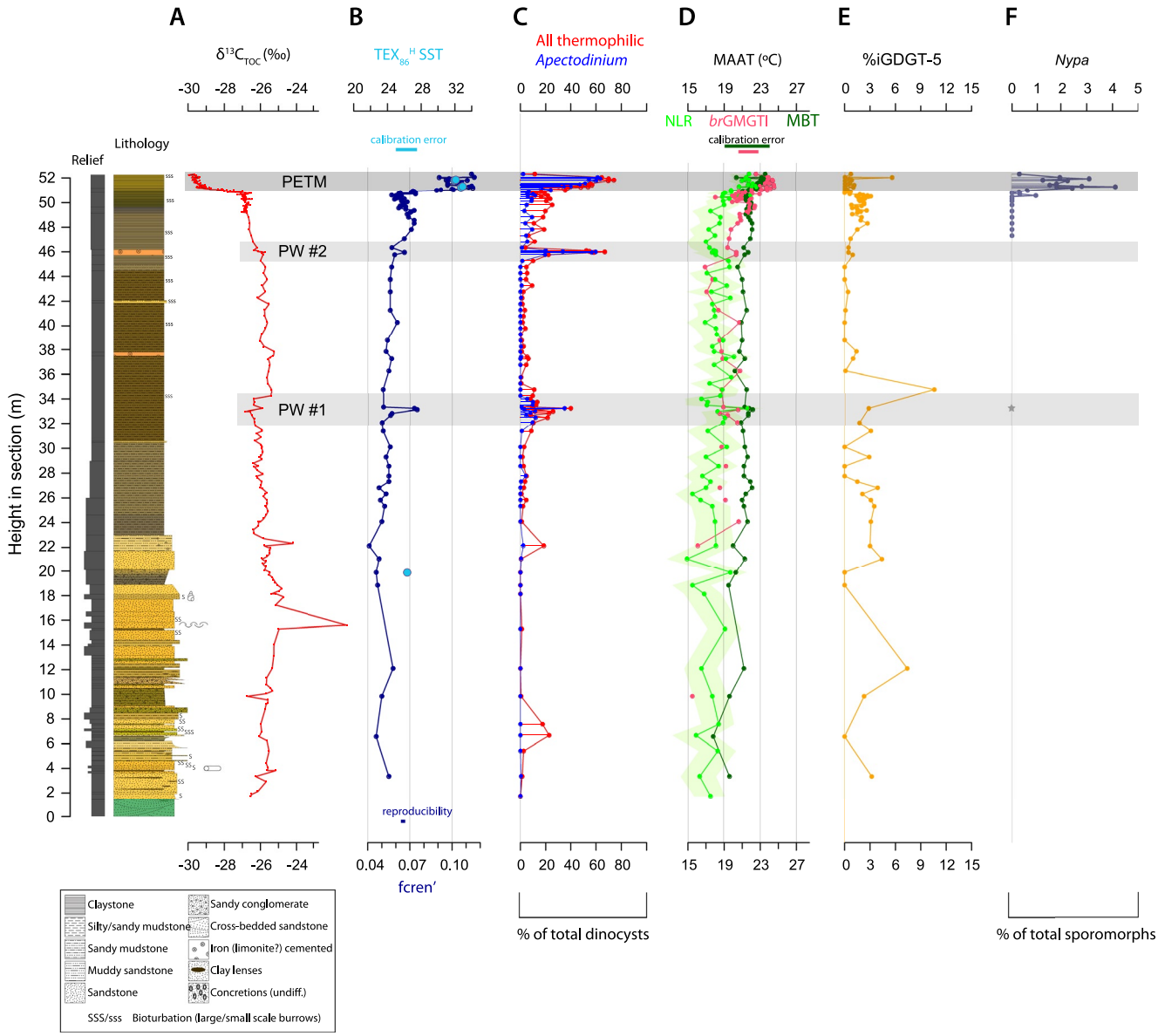

Figure 2. Point Margaret late Paleocene and Paleocene-Eocene Thermal Maximum (PETM) proxy data. (a) Bulk organic matter carbon isotope values ($\delta^{13}C_{TOC}$) and lithology from Frieling et al. (2018). Coloration of lithology indicates approximate sediment color. (b) Sea-surface temperature (SST) trends from relative abundance of crenarchaeol stereoisomer to total crenarchaeol f(cren') and TEX_{86}-based SST estimates. Note that the TEX_{86} data set contains only five samples in total. (c) *Apectodinium* and thermophilic taxa are plotted as % of total dinocyst assemblage. (d) Mean annual air temperature estimates based on MBT'_{5Me}, nearest-living relative (NLR) (Huurdeman et al., 2021 and this study), and brGMGTI (this study). (e) %GDGT-5. (f) *%Nypa* of total pollen and spore assemblage (Huurdeman et al., 2021). PW#1 and #2 refer to pre-cursor warming events.

et al., 2017; Sinninghe Damsté, 2016). Similarly, we calculate the relative abundance of 6-methyl brGDGT isomers using the Isomer Ratio to identify input from fluvial brGDGT-producers (Dearing Crampton-Flood et al., 2021; De Jonge, Hopmans et al., 2014; Sinninghe Damsté, 2016).

2.4.2. brGMGTI and Other brGMGT—Based Proxies

Branched glycerol monoalkyl glycerol tetraethers (brGMGTs) are produced by unknown bacteria and are characterized by an additional covalent C-C bond linking their two alkyl chains (Morii et al., 1998; Schouten et al., 2008). The presence of this bond is thought to improve the stability of the membrane under extreme environmental conditions, such as higher temperature. We identify brGMGT compounds with *m/z* of 1048, 1034, and 1020 (Table 1). In addition to peats (Naafs, McCormick, et al., 2018) and lake sediments (Baxter et al., 2019), these compounds

are also produced and recorded in the marine realm (Liu et al., 2012), particularly in oxygen-minimum zones (Xie et al., 2014). Following the outline in Sluijs et al. (2020), we use the nomenclature of Baxter et al. (2019) to identify the compounds that are used to calculate the brGMGTI and MBT based on H-shaped compounds ($HMBT_{acyclic}$) indices (Baxter et al., 2019; Naafs, McCormick et al., 2018). The %brGMGTs relative to total brGMGTs and brGDGTs, the brGMGTI, and $HMBT_{acyclic}$ have all been proposed as temperature proxies (Table 1). Even though several recent papers have reported the occurrence of these compounds in Paleogene marine sediments (Bijl et al., 2021; Cramwinckel et al., 2022; Sluijs et al., 2020), their deep-time application remains largely untested. We here explore the temperature-proxy potential of brGMGTI, $HMBT_{acyclic}$ and %brGMGTs in our shallow-marine setting (Figure 2, Figures S4–S6 in Supporting Information S1).

2.4.3. TEX_{86}

The degree of cyclization of isoGDGTs produced by marine Thaumarchaeota is captured in the TetraEther index of tetraethers consisting of 86 carbon atoms (TEX_{86}), and can be used to reconstruct SST (Schouten et al., 2002). Prior to calculating TEX_{86}-based temperatures (Kim et al., 2010; Schouten et al., 2002), we test whether the isoGDGT distributions generally align with those observed for the global core-top database used to build the calibration. In this, deviation from the core-top isoGDGT distributions is indicated by a high value of delta ring index (ΔRI). Such differences in isoGDGT distributions might be related to high soil-derived lipid input, which can be assessed using the branched and isoprenoid tetraether (BIT) index (BIT), or to isoGDGT contributions from methanogens and methanotrophs, which can be identified through the methane index (MI) (Hopmans et al., 2004; Weijers et al., 2011; Zhang et al., 2011, 2016). Together, these indices aid in identifying samples in which the isoGDGT composition is altered by non-thermal effects and thus may not yield reliable TEX_{86}-based SST results. For samples that passed the ΔRI cut-off (<0.3), the ratio of GDGT-2 over GDGT-3 (hereafter [2/3]) is employed to assess possible contributions of isoGDGTs derived from deep-dwelling Thaumarchaeota (Table 1, see also Section 4).

2.4.4. f(cren')

f(cren') might be useful to gain insight into SST trends from samples with substantial non-thermal isoGDGT overprints, as identified by ΔRI (Table 1). This is because crenarchaeol is exclusively produced by Thaumarchaeota (De La Torre et al., 2008; Sinninghe Damsté et al., 2002) and therefore substantially less sensitive to overprints by methanogenic or methanotrophic archaea than GDGT-1, -2, and -3 that make up most of the TEX_{86}. Weijers et al. (2006) indeed noted that the abundance of crenarchaeol in soils is relatively low, particularly in more acidic soils.

The temperature dependency of f(cren') may be the result of membrane adaptation within Thaumarcheota populations, as the stereoisomer results in slightly different membrane packing (Bale et al., 2019; Schouten et al., 2013; Sinninghe Damsté et al., 2018). In the natural environment, the temperature dependency may also originate from shifts in the Thaumarcheotal populations, as has been observed in the water column of lake Chala (Baxter et al., 2021). In the latter case, the positive temperature correlation may come from more dominant (sub-)surface-dwelling Thaumarchaeota group I.1b that synthesizes more cren' relative to Thaumarchaeota from group I.1a, for example, due to changing oxygenation, stratification or nutrient distribution within the water column (Baxter et al., 2021). However, strains of Thaumarchaeota group I.1b have so far not been detected in the marine environment.

2.4.5. %iGDGT-5

In addition to the standard marine isoGDGTs that are part of the TEX_{86}, we also calculate the abundance of isoprenoid GDGT-5 as a percentage relative to isoGDGTs 1–3 (Naafs, Rohrssen, et al., 2018). The occurrence of GDGT-5 (>1%) is currently restricted to regions with MAAT of at least 19°C and the compound is found almost exclusively in acidic peats. While %GDGT-5 has been applied to Paleogene lignites (Naafs, Rohrssen, et al., 2018), the proxy has not yet been applied in (shallow) marine settings. While we detect and calculate %GDGT-5 here, we note that %iGDGT-5 in marine settings will be influenced by additional non-peat sources of GDGTs 1–3, such as marine Thaumarchaeota, methanogens and methanotrophs. The calculated %GDGT-5 thus represents a minimum estimate of the %GDGT-5 of the initial peat material.

2.5. Data Compilation for the Southern Ocean

We focus on late Paleocene, PETM and EECO marine and terrestrial temperature proxy records for the Southern Ocean, ranging from New Zealand in the southwest Pacific Ocean in the east to the AAG in the west,

between paleolatitudes of 50°S and 65°S (Müller et al., 2019; Seton et al., 2012) (Figure 1, Table 1). Both quantitative (GDGT-based proxies, foraminiferal Mg/Ca, NLR-based estimates) and semi-quantitative/qualitative (temperature-indicative dinocyst and mangrove palm pollen) temperature information is incorporated. Absolute temperatures are compared within proxies, within the selected time slices. Time-slices "latest Paleocene" (57–56 Ma) and "PETM" (~55.9 Ma) were identified based on carbon-isotope data ($\delta^{13}C$) if available (i.e., for Ocean Drilling Program (ODP) Site 1172 and Deep Sea Drilling Project Site 277) and/or on pollen-based biostratigraphy. We here use records from the upper *Lygistepollenites balmei* zone and the *Spinizonocolpites prominatus* subzone to represent the latest Paleocene and PETM, respectively. Consequently, the included Paleocene data have a maximum age of ~57 Ma (Frieling et al., 2018), in compliance with previous compilations and DeepMIP (Dunkley Jones et al., 2013; Frieling et al., 2017; Hollis et al., 2019). Only data comprising the "body", that is, the stable period of anomalously low $\delta^{13}C$ within the PETM CIE, were used in order to focus on the period of sustained peak warmth. Consequently, the rapid onset and more gradual recovery of the CIE, that is, with $\delta^{13}C$ values, and potentially temperature, intermediate between background and peak PETM values, were not included. A broad interval covering the EECO, ca. 53–49 Ma, as defined by Westerhold et al. (2018) previously identified by bio-, magneto- and isotope stratigraphy is used for the EECO data compilation (Hollis et al., 2019). As it is often challenging to assign absolute ages for terrestrial deposits, we also include localities that were determined to be "Ypresian" and "Early Eocene" in age (Hollis et al., 2019).

3. Results

3.1. Mean Annual Air Temperature Estimates for the Northern Australo-Antarctic Gulf

3.1.1. BrGDGTs

Distributions of brGDGTs in sediments from Point Margaret are generally indistinguishable from those in modern soils and peats, with negligible riverine or marine sedimentary contributions throughout the entire succession (Figure S11 in Supporting Information S1), in line with the findings of Huurdeman et al. (2021) for the top of the succession. We here extended the MBT'_{5Me}-MAAT estimates for the entire late Paleocene part of the Point Margaret section (Figure 2d). There is a long-term warming trend (~4°C) from ~18 to 22°C from the base of the section to the onset of the PETM warming around 50.8 m. We find two minor pre-cursor warming events (PW#1 and PW#2) at ~33 and 46 m superimposed on the long-term trend, which are also supported by f(cren') and dinocysts. The NLR record only shows a response during the first pre-cursor warming (Figures 2b and 2c). Potentially similar fluctuations in MBT'_{5Me} further down the section (e.g., ~27 m, Figure 2d) cannot be confirmed as warming events, as these fluctuations are not mimicked by the trends in other proxies. While the amplitude of these warming events does not exceed the calibration error of the temperature proxies (Figure 2), the analytical precision for the lipid-based parameters (f(cren'), MBT'_{5Me}) is at least an order of magnitude higher and sufficient to detect more subtle temperature signals. While we cannot provide absolute estimates of the magnitude of warming during the events, the correspondence of several proxies and analytical precision of the methods strongly suggests that these periods represent anomalous warming.

3.1.2. Isoprenoid GDGT-5

In the Point Margaret sediments we find high %GDGT-5 (0%–10% Figure 2e). The occurrence and abundance of this compound in our shallow marine setting is likely explained by substantial input of peat-derived material, consistent with the presence of *Sphagnum* spores (Huurdeman et al., 2021). Although there is substantial scatter and a few (n = 13) samples without GDGT-5 throughout the section, GDGT-5 is mostly present (n = 81) and comprises up to ~10% of the isoGDGT assemblage (GDGTs 1–3) (Figure 2, Figure S9 in Supporting Information S1). Such %GDGT-5 values are close to the maximum percentage observed for modern tropical peats (Naafs, Rohrssen, et al., 2018). In the upper part of the section, %GDGT-5 reaches a maximum of 3% on a relatively stable latest Paleocene (43–50 m height) average ~1.5%. In this interval, %GDGT-5 appears to broadly follow the rise and fall in MBT'_{5Me}. However, a correlation between these proxies is absent as the trends in %GDGT-5 and MBT'_{5Me} are stratigraphically offset.

However, as GDGTs 1–3, used to calculate %GDGT-5, are also derived from marine Thaumarcheota and possibly other non-terrestrial sources (Figures S4 and S8 in Supporting Information S1), the calculated %GDGT-5 for all our samples must be regarded as a minimum estimate of the original peat-derived source. Considering that the calculated terrestrial fraction of GDGTs 1–3 is ~30%–50% (Figure S8 in Supporting Information S1) in some

late Paleocene intervals, the relative abundance of GDGT-5 in the source material could well have been similar to, or higher than some modern tropical peats (Naafs, McCormick, et al., 2018; Naafs, Rohrssen, et al., 2018). A single-point within the body of the CIE reaches ~6 %GDGT-5 (Figure 2e). However, it is difficult to gauge the value of this observation: starting from the onset of the CIE, %GDGT-5 and *Sphagnum* spores are no longer consistently present. The erratic occurrence and abundance of GDGT-5 may have occurred through sea level rise so that Point Margaret becomes relatively more distal. GDGT-5-containing terrestrial material is deposited nearer to shore, becomes extremely diluted by marine GDGTs 1–3 or the peat lands are lost as a consequence of warming. The greater abundance of marine dinocysts and lower BIT index values (Figure S9 in Supporting Information S1) and the occurrence of a fern-spike (Huurdeman et al., 2021) in this interval suggests that changes in both the terrestrial and marine realm may have affected the %GDGT-5 record across the PETM in this shallow-marine setting.

3.1.3. BrGMGTs

The Point Margaret section yields a suite of brGMGTs that have recently been documented in mineral soils and river sediment (Kirkels et al., 2022), peats (Naafs, McCormick, et al., 2018; Tang et al., 2021), Paleogene lignites (Naafs, McCormick, et al., 2018), African lakes (Baxter et al., 2019) and both modern marine surface (Liu et al., 2012) and Paleogene marine sediments (Bijl et al., 2021; Cramwinckel et al., 2022; Sluijs et al., 2020). Naafs, McCormick, et al. (2018) show that the relative abundance of brGMGTs over regular brGDGTs is positively correlated with MAAT in peats. In the Point Margaret section, the amount of brGMGTs relative to brGDGTs is positively correlated to MBT'_{5Me}, but is marked by higher values (>10% of total brGDGTs) than all modern peat samples at the same MAAT (Figure S5 in Supporting Information S1). This may indicate that we significantly underestimate absolute temperatures or that additional sources, for example, marine (sedimentary) organisms, add brGMGTs in our setting (Baxter et al., 2021; Kirkels et al., 2022). Baxter et al. (2019) calibrated the brGMGT distributions, formulated as brGMGTI, in tropical lake sediments to temperature. Although the application of the brGMGTI proxy outside tropical lakes is unvalidated, we note that the brGMGT-derived MAAT response at our site follows the trends of other temperature proxy records, although the amplitude is somewhat greater than that based on MBT'_{5Me} (Figure 2d). We also find high scatter in the brGMGTI record in some intervals, particularly around the onset of the PETM CIE, 49–51 m, which may suggest the mixing of different brGMGT sources, likely peat and in situ marine.

Despite the relatively limited range of temperature covered in our data, the $HMBT_{acyclic}$ (Naafs, McCormick, et al., 2018) shows a strong correlation with for example, MBT'_{5Me} and f(cren') (Figure S7, Text S1 in Supporting Information S1). However, accurately assigning variability to either air or SST, or another, indirect control is difficult without proper source identification (Kirkels et al., 2022). Collectively, it is noteworthy that both $HMBT_{acyclic}$ and brGMGTI follow MBT'_{5Me} trends and that brGMGTI produces similar MAAT despite the lack of an environment-specific calibration.

3.1.4. Terrestrial Palynomorphs and NLRs

The expanded late Paleocene record (0–47 m) from Point Margaret yields relatively high MAAT (~18°C) considering its paleolatitude between 55 and 65°S. The late Paleocene NLR-based MAAT of the pollen and spore taxa align well with estimates from the upper part of the Point Margaret section (Huurdeman et al., 2021) and Latrobe-1 (this study). NLR-based MAATs are 17–19.8°C (median: 18.1°C) for the late Paleocene. MAAT estimates from the lower part of section (2–30 m) yield values around 17°C, and slightly higher (~18°C) in the upper part of the succession (30–48 m), with a subtle increase around ~33 m signaling a pre-cursor warming event also observed in brGDGT-based MAAT estimates. The second pre-cursor warming event (~46 m) is not clearly reflected in NLR-based MAAT. A ~3–4°C rise in MAAT was previously calculated for the PETM (Huurdeman et al., 2021).

Aside from the NLR approach to estimate MAAT, we use the well-known climatic envelopes of fossil pollen taxa such as *S. prominatus* (*Nypa*), a mangrove palm that only occurs in regions with MAAT > 22°C at present (Reichgelt et al., 2018). This species has a first consistent appearance at 50.57 m at Point Margaret (Figures 2f), 23 cm below the CIE onset (Huurdeman et al., 2021), and occurs within the PETM CIE body (299.67 m below surface) and the EECO in the Latrobe-1 core. A single occurrence of *Nypa* is registered during the first pre-cursor warming (~33 m). The presence of *Nypa* implies that coastal MAAT was, at times, at least 22°C in the northern AAG just prior to and during the PETM and during the EECO.

3.2. Sea Surface Temperature Estimates for the Northern Australo-Antarctic Gulf

3.2.1. TEX_{86}

We generated isoGDGT data for the Point Margaret outcrop and Latrobe-1 borehole. The isoGDGT distributions in most samples from the Point Margaret section and the Latrobe-1 bore have ΔRI values >0.3 signaling non-pelagic contributions to the isoGDGT pool (Zhang et al., 2016). In most samples, soil-derived isoGDGT input, as indicated by the BIT index and contributions from methanogenic and methanotrophic isoGDGT producers, as derived from the MI exceeded generally proposed cut-offs (0.3 for BIT (Hopmans et al., 2004; Weijers et al., 2007) and 0.3 for MI (Zhang et al., 2011)) (Table 1). GDGT concentrations in the Latrobe-1 samples are <1 ng g^{-1} sediment or <10 mg g^{-1} TOC for most compounds, generally sufficient to identify, but not properly quantify, isoGDGTs, and insufficient to identify penta- and hexamethylated brGDGTs and brGMGTs. This implies that brGDGT distributions could not be used to calculate MBT'_{5Me} and MAAT for these samples. We also note that the recorded GDGT concentrations are remarkably low compared to the sediments from the nearby (~3 km) Point Margaret, which may be the result of oxidation during long-term (40–50 year) dry storage. A similar effect was noted for dinocysts (Frieling et al., 2018).

Further excluding samples with ΔRI > 0.3, only five samples at Point Margaret were identified as suitable to calculate TEX_{86}-derived SST, of which 4 are from the PETM CIE. A single late Paleocene data point with ΔRI < 0.3 yielded a TEX_{86} value of 0.66, and although this sample does pass the ΔRI cut-off, it is marked by a very high BIT index value (0.76). Similarly, two late Paleocene high-BIT index samples from the Latrobe-1 core with low GDGT-3 abundances (<3,000 peak area, typically <0.5 ng g^{-1} sediment for GDGT-3), had otherwise normal isoGDGT-distributions based on ΔRI values (<0.3) and yielded TEX_{86} values of 0.67. However, as the concentrations of most isoGDGTs and brGDGTs approach the analytical limits and potentially have high terrestrial isoGDGT contributions, the resulting TEX_{86} values must be viewed with caution as the analytical error is larger than for other samples and indices. Absolute SST estimates based on TEX_{86}^{H} (Kim et al., 2010) are ~27°C for the late Paleocene and ~32°C during the PETM, implying a 5–6°C warming during the PETM.

3.2.2. f(cren')

In our samples that are marked by very high terrestrial input f(cren') may provide supporting information on relative SST changes. The temperature-dependency of f(cren') is based on the link between temperature and f(cren') in cultures as well as the modern core-top calibration data set (Bale et al., 2019; Kim et al., 2010; Schouten et al., 2002; Tierney & Tingley, 2015). In the core-top data, SST explains a substantial part of the variability in f(cren') (linear $R^2 = 0.6$) in waters with an SST above 10°C, although this is slightly less than the traditional TEX_{86} (linear $R^2 = 0.75$) in the same data set (Schouten et al., 2002; Tierney & Tingley, 2015) (Figure S1 in Supporting Information S1). Moreover, at nearby ODP Site 1172 (Bijl et al., 2021; Sluijs et al., 2011), virtually all variation in TEX_{86} is captured ($R^2 = 0.98$; Figure S3 in Supporting Information S1) by f(cren') across the PETM.

The concentration of crenarchaeol decreases with increasing soil acidity and crenarchaeol rarely exceeds a relative abundance of 10% of isoGDGTs in acidic soils (pH < 6). The same applies to peats and Paleogene lignites, where crenarchaeol rarely exceeds 5% (Naafs, Inglis, et al., 2017; Naafs, McCormick, et al., 2018; Naafs, Rohrssen, et al., 2018). Based on the cyclization of brGDGTs (quantified in the CBT' index; De Jonge, Hopmans et al. (2014); De Jonge, Stadnitskaia, et al. (2014)), we find that soils with low pH (values <5 in Paleocene, ~5.5 during the PETM) dominate the brGDGT distribution at our site (Huurdeman et al., 2021). Collectively, the brGDGTs appear predominantly derived from acidic soils and peats. When we model the contribution of terrestrial isoGDGTs from brGDGT using the approach of Sluijs et al. (2020), we find that the majority of crenarchaeol in our samples is most likely derived from marine Thaumarchaeota and not soils, despite high BIT (Figure S8 in Supporting Information S1).

In the Point Margaret section, we therefore employ f(cren') to assess the temperature trends in the marine realm (Figure 2b). Similar to the data from ODP 1172, in Point Margaret, f(cren') show a correlation with the scarce TEX_{86} data ($R^2 = 0.96$, $p = 0.002$, $n = 5$, Figure S3 in Supporting Information S1) and broadly reproduces the subtle long-term rise in MBT'_{5Me}- and NLR-derived temperatures in the late Paleocene (0–50 m), as well as the two late Paleocene transient precursor warming episodes (~33 and 46 m) (Figures 2b and 2f). The precursor warming events are pronounced in f(cren'), whereas the response in brGDGTs and NLR appears more subdued.

Moreover, f(cren') rises just before (50.57 m) the onset of the CIE (50.8 m), whereas the rise in MBT'_{5Me} slightly lags the CIE (~51 m). SST rise directly prior to the CIE, as recorded here in f(cren'), has also been recognized elsewhere (Frieling et al., 2019; Secord et al., 2010; Sluijs et al., 2007; Thomas et al., 2002). The presumed temperature signal obtained from f(cren') is supported by the coeval, consistent appearance of *Nypa* pollen (Huurdeman et al., 2021, Figure 2f). The delayed response (up to a few kyr) in MBT'_{5Me} compared to vegetation-derived MAAT was attributed by Huurdeman et al. (2021) to (a) differences in transport time and/or (b) reworking of Paleocene or even older soil materials (John et al., 2012) and clay-bound organic matter (Schneider-Mor & Bowen, 2013), including brGDGTs. The different transport time may result in an apparent delay in warming in peat and soil-derived components (brGDGTs, and (peat-derived) brGMGTs). Warming based on above ground vegetation (palynomorphs), especially coastal elements (mangrove palms) and marine compounds (f(cren'), dinocysts), would be more synchronous with the warming. These processes may have also played a role in suppressing the temperature change inferred from MBT'_{5Me} relative to other proxies during the pre-cursor warming events.

3.2.3. Dinocysts

The dinocyst assemblages at Point Margaret are dominated by low-salinity tolerant taxa throughout most of the late Paleocene section (<50 m) (Figure S9 in Supporting Information S1) (Frieling & Sluijs, 2018). Intervals with higher abundances of inner-neritic or coastal taxa are also recorded, likely signaling periods of diminished freshwater influx. Thermophilic dinocyst taxa, here mainly *Apectodinium*, become regular constituents of the assemblage around ~26 m and open marine taxa (e.g., *Spiniferites* spp.) are progressively more abundant upsection and suggest more distal or open marine conditions.

The late Paleocene and PETM SST trends as reconstructed through f(cren') are supported by progressively higher percentages of thermophilic dinocysts toward the top of the Paleocene section (Figure 2c), even though these taxa are outnumbered by low-salinity tolerant taxa during pre-CIE warming and onset of the PETM CIE (ca. 50–50.9 m, Figure S9 in Supporting Information S1). In addition to rough trends, the appearance and relative abundance of selected extinct thermophilic dinocysts, notably *Apectodinium* spp. and *F. reichartii* provide constraints on minimum SST (Frieling & Sluijs, 2018). The first abundance events of *Apectodinium* (>10%) are found during the precursor warming events in the latest Paleocene (at ~33 and ~46 m, Figure 2c) at Point Margaret. These events are not registered in the Latrobe-1 core, which may be due to low sampling resolution and/or poor recovery in the respective core intervals. A third abundance increase is recorded at Point Margaret during the CIE, which is mirrored by a similar event in the Latrobe-1 core (Figure S10 in Supporting Information S1). *F. reichartii* is never abundant (maximum: 5% at Point Margaret), and occurs consistently only during peak CIE. A single late Early Eocene (EECO) abundance event of *Apectodinium* is found in the Latrobe-1 core. Following observations of Frieling and Sluijs (2018) we arrive at most likely minimum SST estimates ~20–25°C for the latest Paleocene (based on occasional *Apectodinium* abundance; Latrobe-1 core and Point Margaret), 25–30°C for the PETM (based on *F. reichartii*) for the Point Margaret section and 20–25°C for the EECO in the Latrobe-1 core. At Point Margaret, the relative abundance of these thermophilic taxa follows the long-term late Paleocene SST rise, as well as short-term variations (Figure 2) observed in other temperature proxies (f(cren'), MBT'_{5Me}, brGMGTI) in detail except for a short interval around the CIE onset. The broad patterns in thermophilic dinocysts and fcren' seem to be confirmed by the limited Latrobe-1 core data (Figure S10 in Supporting Information S1), with the note of caution that both the dinocyst and lipid biomarker record may be compromised by degradation during core storage.

3.3. Integrated Regional SST for the Australo-Antarctic Gulf and SW Pacific

The early Paleogene climate of the SW Pacific has been intensely studied with a range of proxies (Hollis et al., 2019). The majority of SST data is based on TEX_{86}, and second planktonic foraminiferal Mg/Ca ratios. Briefly, the SW Pacific TEX_{86}^{H} and Mg/Ca records show SSTs of ~26–30°C in the late Paleocene (Table 2), rising to 31–33°C during the PETM. For the EECO, results are somewhat more variable and carbonate-based proxies show somewhat lower temperatures on average (~26°C) compared to TEX_{86}^{H} (31–32°C) (Hollis et al., 2019).

Fewer data were available for the AAG and prior to this study, none for the late Paleocene and PETM. Although some caution is warranted due to high BIT in our samples, the new data suggest that TEX_{86}-based SSTs in the late Paleocene (27°C), PETM (~32°C) and the published data from Site U1356A (32°C) were indistinguishable from those in the SW Pacific in the same intervals.

Table 2
From Top to Bottom—Sea-Surface Temperature, Mean Annual Air Temperature and Semi-Quantitative Minimum Temperature Proxy Estimates for the SW Pacific and AAG

SST Proxy estimates			Late Paleocene			PETM			EECO			
Region	Site	Proxy	*n*=	Mean	SE	*n*=	Mean	SE	*n*=	Mean	SE	Reference
SW Pacific	Site 1172	TEX_{86}^{H}	0	25.9	0.2	8	31.5	0.3	15	30.9	0.3	Bijl et al. (2009), Bijl, Bendle, et al. (2013), Bijl, Sluijs, et al. (2013), Bijl et al. (2021), and Sluijs et al. (2011)
		TEX_{86}-linear	30	27.2	0.2	8	35.1	0.6	15	34.2	0.5	
	Mid-Waipara	TEX_{86}^{H}				2	33.2	0.8	5	31.6	0.3	Pancost et al. (2013) and Hollis et al. (2012)
		TEX_{86}-linear							5	35.3	0.5	
		Mg/Ca *Acarinina*							4	26.3	1.3	
	Hampden Beach	TEX_{86}^{H}							8	31.9	0.5	Hollis et al. (2009), Hines et al. (2017), and Inglis et al. (2015)
		TEX_{86}-linear							8	35.9	0.8	
		Mg/Ca *Morozovella*							5	28.6	0.9	
		Mg/Ca *Acarinina*							3	26.6	1.8	
	Site 277	Mg/Ca *Morozovella*				7	31.4	0.6	5	29.3	1.4	Hollis et al. (2015) and Hines et al. (2017)
		Mg/Ca *Acarinina*	8	29.8	0.5	8	30.9	0.6	6	31.2	0.4	
	Tora	Mg/Ca *Morozovella*							6	25.7	0.9	Hines et al. (2017)
		Mg/Ca *Acarinina*							6	26.8	1.7	
	Tawanui	Mg/Ca *Morozovella*							1	27.2		Hines et al. (2017)
		Mg/Ca *Acarinina*							1	25.6		
Autralo-Antarctic Gulf	Site U1356A	TEX_{86}^{H}							131	31.9	0.1	Bijl, Bendle, et al. (2013) and Bijl, Sluijs, et al. (2013)
		TEX_{86}-linear							131	35.7	0.1	
	Latrobe-1	TEX_{86}^{H}	2	27.3	0.2							This study
		TEX_{86}-linear	2	29	0.3							
	Point Margaret	TEX_{86}^{H}	1	26.3		4	32.4	0.2				This study
		TEX_{86}-linear				4	36.5	0.4				

MAAT Proxy estimates			Late Paleocene			PETM			EECO			
Region	Site	Proxy	*n*=	Mean	SE	*n*=	Mean	SE	*n*=	Mean	SE	Reference
SW Pacific	Site 1172	MBT							9	21.9	0.1	Bijl, Bendle, et al. (2013), Bijl, Sluijs, et al. (2013), and Bijl et al. (2021)
		NLR	8	14.1	0.8	3	17.4	3.0				Contreras et al. (2014)
	Mid-Waipara	MBT				2	21.2	1.5	6	20.8	0.4	Pancost et al. (2013)
		Coexistence							1	20.0		
	Konkon-1	NLR	3	16.5	1.1	2	21.4	0.2				Contreras et al. (2014)
	Poonboon-1	NLR	3	15.9	0.3	1	19.2					Contreras et al. (2014)
	Cambalong creek	NLR	1	18.5								Greenwood et al. (2003) and Contreras et al. (2014)
		LM	1	13.5								

Table 2
Continued

MAAT Proxy estimates			Late Paleocene			PETM			EECO			
Region	Site	Proxy	*n*=	Mean	SE	*n*=	Mean	SE	*n*=	Mean	SE	Reference
Australo-Antarctic Gulf	Point Margaret	NLR	66	17.9	0.2	8	21.7	0.2				Huurdeman et al. (2021) and this study
		MBT	70	21.3	0.1	12	22.9	0.3				Huurdeman et al. (2021) and this study
		brGMGTI	*58*	*19.7*	*0.2*	12	23.6	0.2				This study
	Latrobe-1	NLR	6	19.7	0.1	1	22.3					This study
	Site U1356A	MBT							62	20.1	0.2	Pross et al. (2012)
		NLR							81	18.4	0.1	
	Lowana Road, Tasmania	Coexistence							2	23.4	0.7	Carpenter et al. (2012)
		Podocarpus leaf length							1	24.3		
		NLR							1	20.0		Reichgelt et al. (2022)
	Deans Marsh	Climate Leaf Analysis Multivariate Program (CLAMP)							1	22.6		Reichgelt et al. (2022)
		NLR							1	19.5		Reichgelt et al. (2022)
	Dinmore	CLAMP							1	19.7		Reichgelt et al. (2022)
		NLR							1	18.9		Reichgelt et al. (2022)

Semi-quantitative temperature estimates			Late Paleocene	PETM	EECO	
Region	Site	Proxy	Minimum	Minimum	Minimum	Reference
SW Pacific	ODP1172	Dinocysts	20	25	25	Sluijs et al. (2011) and Bijl et al. (2021)
		Pollen		22		Contreras et al. (2014)
	Mid-Waipara	Dinocysts		20		Crouch et al. (2014) and references therein
	Tawanui	Dinocysts		20		Crouch et al. (2014) and references therein
	Kumara-2	Dinocysts		20		Crouch et al. (2014) and references therein
	Toi-Flat-1	Dinocysts		20		Crouch et al. (2014) and references therein
Australo-Antarctic Gulf	Point Margaret	Dinocysts	20	25		This study
				22		Huurdeman et al. (2021)
	Latrobe-1	Pollen Dinocysts Pollen	20	25	20	This study
				22	22	This study
	Lowana Road, Tasmania	Pollen and Macrofossils			22	Carpenter et al. (2012)
	U1356A	Dinocysts			20	Bijl, Bendle, et al. (2013), Bijl, Sluijs, et al. (2013)

Note. Data sources: (Bijl, Bendle, et al., 2013; Bijl et al., 2009, 2021; Carpenter et al., 2012; Contreras et al., 2014; Crouch et al., 2014; Greenwood et al., 2003; Hines et al., 2017; Hollis et al., 2009, 2012, 2015; Huurdeman et al., 2021; Inglis et al., 2015; Pancost et al., 2013; Pross et al., 2012; Reichgelt et al., 2022; Sluijs et al., 2011). TEX_{86}-linear refers to the calibration of O'Brien et al. (2017).

This is supported by semi-quantitative lines of evidence, particularly the occurrence and abundance of thermophilic dinocysts; the abundance of *Apectodinium* and occurrence of *F. reichartii* during the PETM are mirrored east and west of the TG (Figures 3 and 4). Similarly, high SSTs during the EECO of Site U1356 are accompanied by high relative abundances of *Apectodinium*.

3.4. Integrated Regional Mean Air Temperatures for the Australo-Antarctic Gulf and SW Pacific

Available late Paleocene MAAT reconstructions for the SW Pacific region are mostly derived from vegetation-based (e.g., NLR, leaf-margin analyses) approaches. MAATs have been reconstructed for several localities, but, due to the nature of the proxies, MAAT is available for a relatively small number of samples per location compared to SSTs. Localities include Konkon-1 and Poonboon-1 in the Bass Basin (e.g., Contreras et al., 2014), and Cambalong Creek, on the southeast Australian coast (Greenwood et al., 2003) (Figure 1), Site 1172 and Mid-Waipara, New Zealand, which together arrive at an average of ~16°C, with MAAT rising to ~20°C during the PETM. The EECO MAAT estimates are based on MBT'_{5Me} from Site 1172 (Bijl, Bendle, et al., 2013; Bijl et al., 2021) and Mid-Waipara (Pancost et al., 2013), and yield MAAT of ~21–22°C.

Within the AAG realm, late Paleocene MAAT reconstructions are now available for the Point Margaret outcrop (Huurdeman et al., 2021; this study) and Latrobe-1 (this study). The abundance of GDGT-5 in the uppermost Paleocene of the Point Margaret outcrop indicates MAAT > 19°C, the NLR-based estimates (Latrobe-1 & Point Margaret) are 16–19°C, and the Point Margaret MBT'_{5Me} estimates are 21–22°C. Both NLR and MBT'_{5Me} indicate a MAAT rise during the PETM to 20–22°C and 23°C, respectively. BrGMGTI derived MAAT estimates suggests slightly higher temperatures during the PETM (~24°C) and a temperature increase comparable to NLR-based estimates (~4°C), although these results should be treated with some caution, as brGMGTI estimates were only calculated for Point Margaret and this novel proxy remains unvalidated in Paleogene marine settings. MAAT estimates for the EECO are derived from only few localities (Table 2). This includes Lowana Road, also known as Regatta Point, in the Sorrell Basin, western Tasmania, Site U1356A on the Antarctic Margin and two recent ensemble (NLR and leaf-morphology) estimates from Dinmore and Deans Marsh, Australia (Reichgelt et al., 2022) (Table 2). The localities show somewhat divergent plant-based MAAT estimates; NLR shows MAAT ~18°C at Site U1356A, while a higher MAAT is reconstructed for Lowana Road (~24°C). The ensemble MAAT estimates from Dinmore and Deans Marsh fall between these estimates. MBT'_{5Me} estimates from Site U1356A align with the average of all vegetation-based estimates (~20–21°C). Similar to the SST estimates, MAAT estimates from the SW Pacific and AAG within the same proxy are indistinguishable for the same intervals.

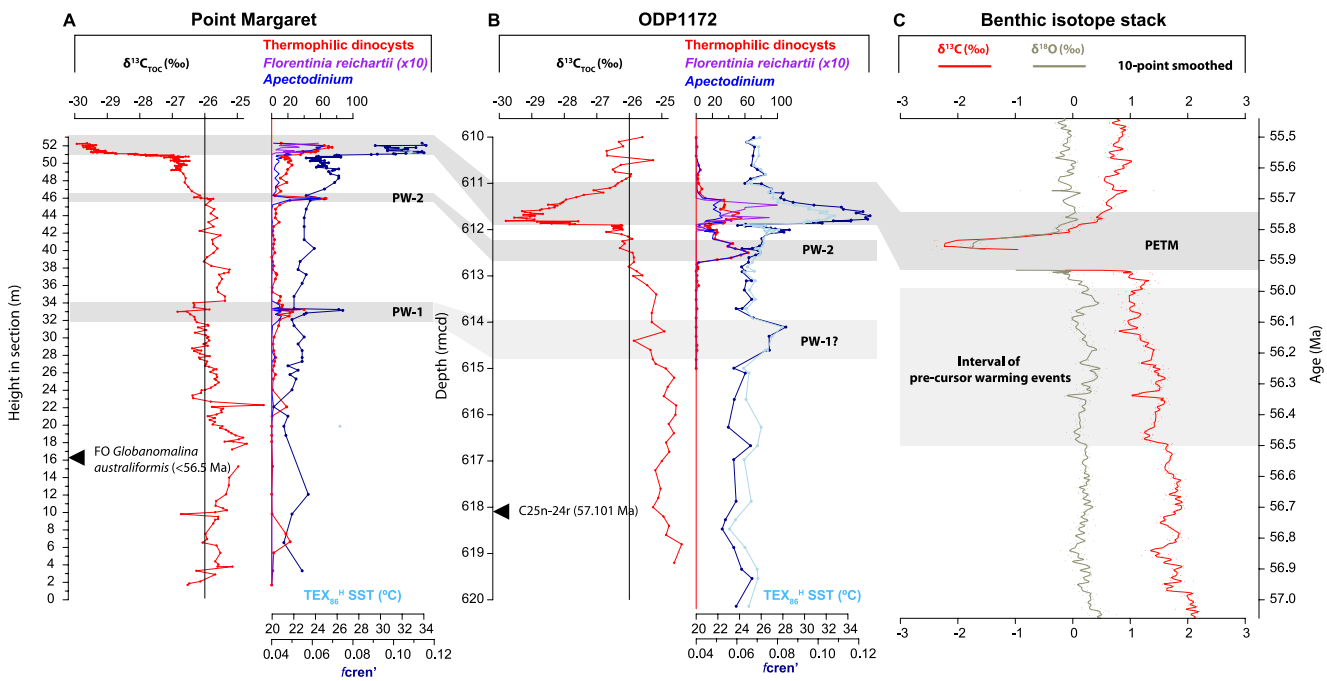

Figure 3. Comparison of latest Paleocene—Paleocene-Eocene Thermal Maximum (PETM) temperature trends west and east of the Tasmanian Gateway. (a) Point Margaret. (b) ODP Site 1172 (data from Bijl et al., 2021; Sluijs et al., 2011). (c) Global deep ocean carbon and oxygen isotope stack based on benthic foraminifera (Westerhold et al., 2020). Events were correlated based on succession of dinocyst events and the PETM carbon isotope excursion (CIE) (~56 Ma) and absolute dates from Point Margaret (first occurrence of *G. australiformis*; (Frieling et al., 2018)) and magnetochron C25n-C24r reversal at Site 1172 (Bijl et al., 2021). Note that sea-surface temperature at Point Margaret is represented by only five TEX_{86} estimates, four within the body of the CIE and one in the late Paleocene. Relative abundances for thermophilic dinocysts and *Apectodinium* are given in % of total dinocysts. The rarer *Florentinia* is plotted amplified 10-fold.

Terrestrial micro- and macrofossil evidence yields a very similar picture: mangrove palm pollen (*Nypa*) are found throughout the entire studied area during the PETM (Figure 4) and also appear during the EECO (e.g., Latrobe-1 core and Lowana Road (Carpenter et al., 2012)).

4. Discussion

4.1. Late Paleocene Warming Events

Multiple, independent, temperature proxies reflect two late Paleocene transient warming events superimposed on subtle or step-wise long-term warming (Figure 2). While the amplitude of warming does not exceed the calibration error for some proxies (NLR, MBT'_{5Me}), the correspondence between the various proxies gives confidence these intervals represent pre-cursor warming events. Importantly, these events do not seem to be local.

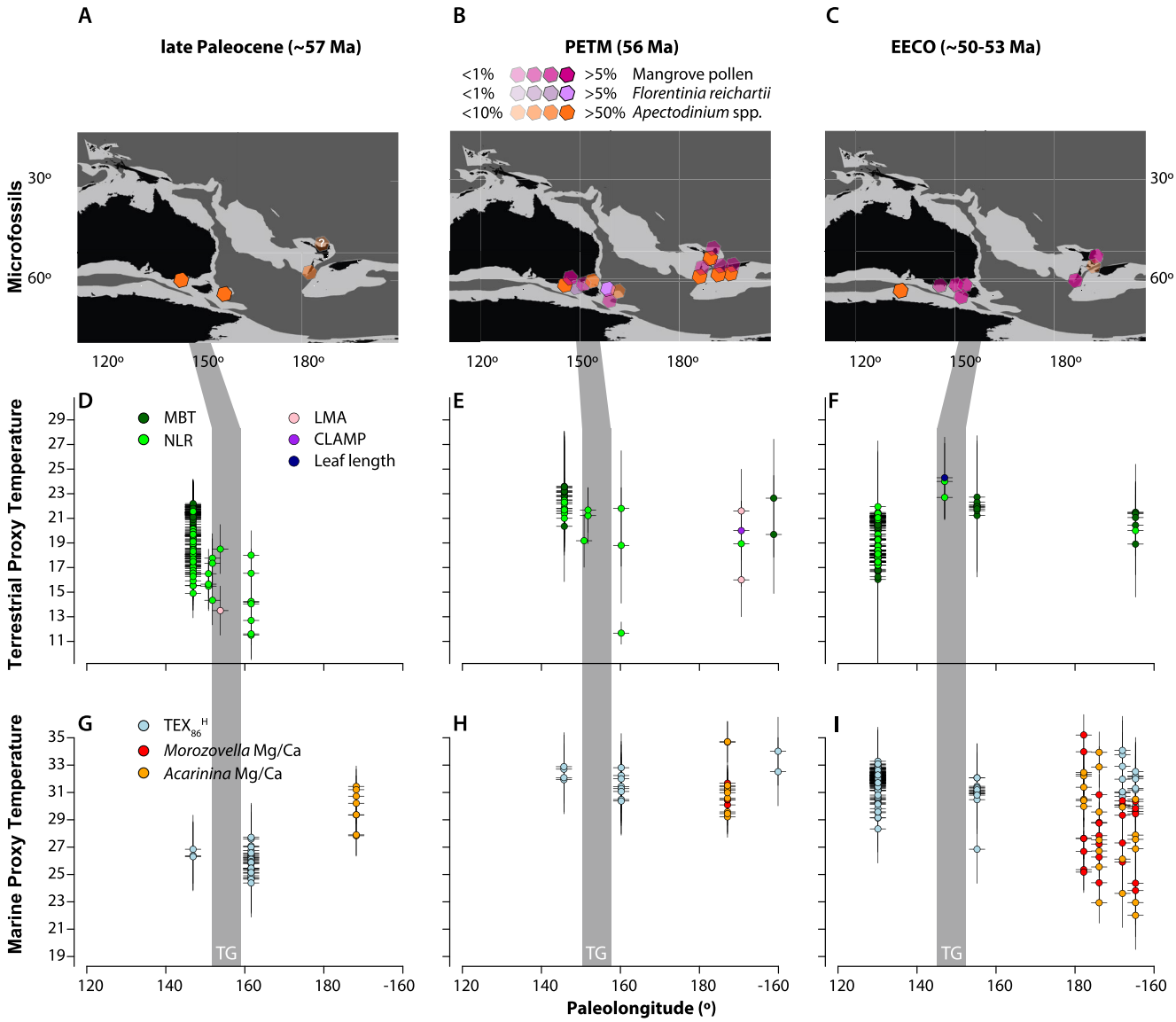

Figure 4. Proxy compilation across three time-slices; late Paleocene, Paleocene-Eocene Thermal Maximum and Early Eocene Climatic Optimum. (a–c) Relative abundance of thermophilic microfossil taxa, mangrove pollen (*Nypa*) and dinocysts (*Apectodinium* and *Florentinia reichartii*), (d–f) Terrestrial temperature reconstructions based on vegetation (dark green) and biomarkers (green). (g–i) Sea-surface temperature reconstructions using TEX_{86}^{H} (light blue), Mg/Ca of mixed-layer foraminifera *Acarinina* (orange) and *Morozovella* (red). Gray vertical band represents the Tasmanian Gateway area. Error bars on temperature reconstruction data represent calibration errors (TEX_{86}^{H} = 2.5°C, Mg/Ca = 1.3°C, MBT'_{5Me} = 4.8°C, nearest-living relative, CLAMP and leaf length = variable).

The second precursor warming (PW-2) at ~46 m in the Point Margaret section has an equivalent at Site 1172 (Figure 3). This may also hold true for the event at ~33 m, although at Site 1172 only very subtle increases in *Apectodinium* abundance (~614.5 m below sea floor) are registered (Bijl et al., 2021). Available bio- and magnetostratigraphic age-depth tie points indicate average late Paleocene accumulation rates were 0.6 cm kyr^{-1} (Sluijs et al., 2011) at Site 1172 and ~7 cm kyr^{-1} (Frieling et al., 2018) Point Margaret. Based on these values, PW-2 may precede the PETM by some 100 kyrs. By extrapolation this would imply that PW-1 at 33 m is another ~200 kyr older, but we note that in marginal settings sedimentation rates can strongly vary on short timescales. Notably, the second precursor warming interval coincides with an increase in open marine and thermophilic dinocyst percentages at the expense of low-salinity tolerant taxa. This suggests more distal conditions or reduced fresh water and siliciclastic flux (Figure 2, Figure S9 in Supporting Information S1). It thus seems likely the second precursor warming interval (PW#2, Figure 2) at Point Margaret represents a period of sediment starvation resulting in a condensed section. At the equivalent level, a distinctly more open marine dinocyst signal is also seen at Site 1172 and no sediment starvation is apparent there. This implies the warming signal appears independent of fluctuations in sedimentation.

Although their exact timing remains unclear, both pre-cursor warming events fall within in an interval with minor deep ocean carbon isotope fluctuations (Cramer et al., 2003; Westerhold et al., 2018, 2020) (Figure 3c). Given current constraints on their age, PW#1 and #2 appear to precede previously recognized precursor carbon isotope events that occur closer (<100 kyr) to the PETM CIE (e.g., Babila et al., 2022; Bowen et al., 2015). Although the raw data suggests that a subtle decrease in $\delta^{13}C_{org}$ co-occurs with the precursor warmings, this could also result from coeval small changes in organic matter sourcing. We find a greater proportion of marine dinocysts as well as slightly lower BIT index values during these events (Figure S9 in Supporting Information S1), which is particularly relevant as a higher proportion of marine organic matter could skew $\delta^{13}C_{org}$ to more depleted values (Sluijs & Dickens, 2012). Therefore, evidence for any CIE occurring at the same level as either of the transient precursor warming events is weak. However, as small $\delta^{13}C$ fluctuations are notoriously difficult to detect in organic carbon we cannot exclude a relation between deep-ocean events and the pre-cursor warming events.

Even if the relation of these subtle transient warming events to the variability recorded in the deep ocean is difficult to constrain, the existence of such events is noteworthy as they exceed the (regional) variability observed in most of the Paleocene (Figure 2). Although these events can only be revealed in high-resolution data generated for background climates, such data is currently scarce. Yet, resolving such signals from background noise could prove essential to understand (Paleogene) climate and carbon cycle behavior (Armstrong McKay & Lenton, 2018; Bowen et al., 2015; Sluijs et al., 2007).

4.2. Potential for brGMGT Proxies

Collectively, we find that the strong correlations with other reconstructed environmental parameters including MAAT and SST support a temperature-related response in brGMGTs. However, their common presence in lakes, peats and marine sediments implies that it is challenging to accurately assign observed variability to either air or SST, or other parameters indirectly related to temperature (Kirkels et al., 2022). Despite this, we note that both HMBT and brGMGTI follow MBT'_{5Me}-based MAAT trends and brGMGTI produces similar absolute MAAT estimates despite the lack of an environment-specific calibration.

Intriguingly, the HMBT not only corresponds in trend with MBT'_{5Me}, but the ratios between the compounds ($HMBT_{acyclic}$; H1020c/H1020c + H1034a + H1048) are also virtually identical to $MBT_{acyclic}$ (defined as brGDGT-Ia/brGDGT-Ia + IIa + IIIa, Table 1), supporting the notion that these compounds have a shared origin and/or mechanistic purpose in microbial membranes. In addition, the increase in brGMGT abundance relative to that of regular brGDGTs (%brGMGT) across the onset of the CIE may imply that the formation of H-shaped compounds represents an additional temperature adaptation (Morii et al., 1998; Naafs, McCormick, et al., 2018) and/or that production of brGMGTs increased relative to that of brGDGTs in specific (i.e., marine) source areas (Kirkels et al., 2022). Despite these unknowns, the clear correlation to reconstructed environmental parameters and the ubiquitous presence of brGMGTs in these (shallow) marine settings such as sampled at Point Margaret highlight the potential for new paleoenvironment proxies based on brGMGTs once their origin and function are better resolved.

4.3. No Temperature Differences Between the Australo-Antarctic Gulf and the Southwest Pacific?

Within proxies, we find that absolute temperatures are within calibration error east and west of the TG. Moreover, marine and terrestrial temperature trends in the AAG and the SW Pacific seem similar for all analyzed intervals (i.e., late Paleocene, PETM and EECO; Figure 4). While paleolatitude is similar, the AAG and SW Pacific are thought to be affected by very different surface ocean currents (Figure 1). It is difficult to reconcile with the proposed large-scale ocean circulation patterns, that is, the warm low-latitude Proto-Leeuwin Current in the AAG and cooler higher-latitude Tasman Current in the SW Pacific, across the analyzed interval (Figure 1). It also contrasts with modeled differences in SST and MAAT between the areas east and west of the TG.

It is remarkable that not only the trends (Figure 3), but also the reconstructed absolute TEX_{86}-based temperatures are similar across analyzed sections in the marine realm (Figure 4). While a seasonality bias in SST proxies could affect latitudinal gradients through dominance of warm-season productivity at higher latitudes (e.g., Antoine et al., 1996), it is unlikely that such effects would eliminate zonal differences (Figure 4). Modern examples, such as the SST difference between the eastern and western North Atlantic that can exceed 5°C (e.g., Gouretski & Koltermann, 2004), support the notion that substantial zonal differences, such as those expected across the TG, should be detectable in proxy data.

One aspect that warrants further exploration is the contribution of deep-water derived isoGDGTs and their potential impact on TEX_{86}-derived temperature reconstructions. While isoGDGT-producing Thaumarcheota occur through the entire water column, their highest concentrations are generally found near the lower part of the mixed layer, in the nitrite maximum, around 50–150 m depth (e.g., Hurley et al., 2016, 2018; Pitcher et al., 2011). The contribution of deep-water derived isoGDGTs can be assessed using [2/3] (e.g., Hurley et al., 2018; Kim et al., 2015; Taylor et al., 2013) (Table 1), which is based on the observation that [2/3] in suspended particulate matter increases rapidly below 150–200 m depth ([2/3] of ∼3 up to ∼200 m depth, ∼25 at >200 m depth) (e.g., Hernández-Sánchez et al., 2014; Hurley et al., 2018). Low [2/3] are observed for the TEX_{86} data sets used here: Point Margaret (average 2), Site 1172 (2.5–3.5 for Paleocene-Eocene, 2.6 for EECO), Mid-Waipara (2.5), Hampden Beach (1.6) and Site U1356 (1.6), which, at face value, suggests contribution of deep-water derived isoGDGTs were minor. We therefore find [2/3] patterns between the localities used here do not reveal any obvious differences in isoGDGT production depths.

The reconstructed temperatures and trends for the AAG relative to those in the SW Pacific increase the geographical extent of the discrepancy between modeled and proxy-derived temperatures in the high southern latitudes (Hollis et al., 2012; Lunt et al., 2021). At the same time, the findings for the AAG imply that the model-data discrepancy is not limited to the SW Pacific, but extends into the AAG (Lunt et al., 2021). Moreover, this zonal pattern did not notably change during intervals of both transient (PETM) and multi-million-year global warming (Late Paleocene-EECO). The temperature patterns exist within the marine and terrestrial realms and are evident in fundamentally different proxies for both realms. This reinforces the existence of anomalously high SSTs in the AAG and particular the SW Pacific and it appears unlikely that the discrepancy can be resolved by an improved mechanistic understanding of a single SST proxy. While the proxy-derived MAAT for both regions is within calibration error, the absolute reconstructed MAATs are often ca. 10°C below SST (see also e.g., Bijl et al., 2021) and in relatively close agreement with modeled MAAT at high pCO_2 (e.g., Lunt et al., 2021; Reichgelt et al., 2022).

It remains uncertain how accurate the reconstructed absolute mean annual temperatures from the individual proxies are. For example, culture experiments emulating the non-analog high-latitude conditions, such as the seasonal contrasts in light conditions in combination with high-temperature, are yet lacking. Constraining proxy behavior under climate conditions such as those that prevailed in the high southern latitudes during the early Paleogene might prove crucial to assess the value of currently available and forthcoming data. In the following section, we explore and revisit new and previously proposed options that may merit further attention in order to improve our understanding of deep-time high-latitude climate.

4.4. Spatial Biases in the Proxy and Modeled Temperature Signals

In general, the inherent heterogeneity of hinterlands and, by extension, sourcing and transport of terrestrial components, particularly pollen and spores, gives rise to several challenges and may complicate a robust comparison between localities (e.g., Inglis et al., 2019). Challenges include changes in the catchment area, including

vegetation source, river flow path, coastal proximity, altitude, and spatial integration. While this may affect some interpretations that rely on whole assemblages or presence/absence data (NLR), we suggest that this is likely a relatively minor issue for lowland or coastal taxa and indeed much of the study area. We find that this assumption is warranted by the apparently synchronous appearance of *Nypa* across the TG, the relatively short time span of the studied time interval, and the fact that all records come from passive margins, implying that major tectonic changes in the catchment area are unlikely. However, comparing to localities further offshore or regions with strong (paleo)relief will invariably include some of these factors.

As the above factors mostly affect terrestrial proxy data, it is unlikely that invoking one single effect (e.g., seasonal biases, sourcing) resolves much of the model-data discrepancy. However, until recently, one effect on marine temperature proxies may have been largely overlooked. There is a dominance of records from near-shore, shallow and coastal environments in the compilation, an inherent (preservation) bias of many deep-time temperature reconstructions. Modern marginal marine settings generally experience greater influence of nearby landmasses and, partly as a consequence, more pronounced seasonal SST variations (~10°C) compared to open marine or oceanic (typically <5°C) (Hirahara et al., 2014; Judd et al., 2020), and it is reasonable to assume that this was similar in the Paleogene. A greater mean annual temperature range potentially exacerbates any seasonal bias that may exist in proxy data for example, by further amplifying warm-season dominated proxy signals.

Lastly, the low-resolution (1° and greater) models the (paleo)climate modeling community relies on tend to strongly over- or underestimate temperature in specific regions due to lack of fine-scale oceanographic features such as meso-scale eddies. The effects of this are most pronounced in regions associated with eastern and western boundary currents (Judd et al., 2020). Comparing the mostly nearshore paleoclimate reconstructions to low horizontal resolution model simulations may be complicated by such effects (Judd et al., 2020; Nooteboom et al., 2022), especially for regions with complex (paleo)geography. As these factors are challenging to constrain and the impact is likely to be site-specific it is difficult to gauge whether and how this may influence our ability to constrain and compare regional temperature patterns.

4.5. Influence of Paleogeography

On a global scale and over latitudinally averaged zones, climate models can now reproduce Eocene proxy data (Cramwinckel et al., 2018; Evans et al., 2018), but an accurate representation of the global, local and regional paleogeography becomes important for finer-scale model-data comparisons (Frieling et al., 2017; Lunt et al., 2016; Nooteboom et al., 2020, 2022). The paleogeography of the region around the TG includes many continental blocks of uncertain paleobathymetry (S. E. Williams et al., 2019), which means that even if fully coupled simulations were to be run in higher spatial resolution, substantial uncertainties in paleobathymetry/paleogeography may still impact temperature distribution. However, extreme end-member early Paleogene (prior to ca. 50 Ma) TG geographies with either deep throughflow or high topography have predictable climatic and oceanographic consequences (Bijl et al., 2011; Sauermilch et al., 2021; Sijp et al., 2011, 2016) that remain unsupported by the combination of tectonic, biogeographic and temperature proxy data (Baatsen et al., 2018). This implies that such drastic changes in paleogeographic boundary conditions are not primary candidates to resolve the regional discrepancy between data and models.

Although the paleobathymetry of the SW Pacific itself has received less attention than Southern Ocean gateways (Bijl, Bendle, et al., 2013; Lagabrielle et al., 2009; van de Lagemaat et al., 2021), recent work has suggested that sectors of the now submerged continental plates of Zealandia may have been shallow or even emerged above sea level during the Paleogene (Sutherland et al., 2019). The exact influence of bathymetric features on the surface and deep ocean flow and heat distribution in this region is yet unknown, but likely important for the exact configuration and shape of the South Pacific polar gyre and thereby the direction of the Proto-East-Australian Current, as has been argued for other regions of deep-water formation (Coxall et al., 2018; Vahlenkamp et al., 2018).

Apart from regional or local details in paleogeography, the use of either a hotspot or paleo-magnetic reference frame for absolute paleolatitude reconstructions may have a large impact on modeled oceanography at the sites used in this study. The type of framework does not notably affect the positions of the sites relative to each other, but the paleomagnetic framework shifts localities around the TG ca. 5 (±5)° latitude north (Müller et al., 2019; Seton et al., 2012; van Hinsbergen et al., 2015), relative to the spin axis of the Earth. While this may seem trivial, much of the region is within a latitudinal band that is highly sensitive to such changes (Baatsen et al., 2020). Specifically, placing the same regional geography at lower latitudes implies that there is a higher probability

of wind-driven surface currents entering the AAG and the SW Pacific through the Proto Leeuwin Current and Proto East-Australia Current, respectively, an effect that is independent of model resolution (Baatsen et al., 2018; Nooteboom et al., 2022). Ultimately, the minor shifts in paleolatitude may therefore have major impact on the origin and temperature of water masses bathing sites east of the TG.

4.6. Low-Latitude Current Invasion Into the SW Pacific and Australo-Antarctic Gulf

Intriguingly, recent high-resolution (0.1°) ocean model simulations show an invasive Proto East-Australia current in the middle Eocene, penetrating as far south as ~55°S (Nooteboom et al., 2022), bringing it within reach of some SW Pacific sites (e.g., Site 277, New Zealand) unlike previous simulations (e.g., Hollis et al., 2012; Huber et al., 2004). A shallow connection between the AAG and the SW Pacific may have existed in the early Paleogene and would be in line with a superficial similarity of the dinocyst assemblages from Site 1172 and Point Margaret and Latrobe-1. However, dinocyst bioprovinces are generally not well-defined in the Paleocene and earliest Eocene, with the majority of taxa likely having a cosmopolitan distribution (e.g., Frieling & Sluijs, 2018), implying similarity on either side did not necessitate an open TG and associated warm or cold through flow.

While the observed biogeographic separation in the Middle and Late Eocene (Bijl et al., 2011; Cramwinckel et al., 2020; Huber et al., 2004) may be interpreted as the expression of a temperature or oceanographic difference, most modern and extinct dinocysts, including thermophilic taxa such as *Apectodinium* have a wide temperature tolerance (Frieling & Sluijs, 2018; Prebble et al., 2013; Zonneveld et al., 2013). Therefore, it is much more likely that a combination of local environmental parameters, including, for example, nutrient availability, coastal proximity and salinity (Bijl et al., 2021), ultimately determined the assemblage characteristics and therefore regional biogeography (Bijl et al., 2011; Zonneveld et al., 2013). In this sense, previous interpretations of corresponding modeled high or low SST and biogeography may have overstated the influence of SST on dinocyst biogeography.

With the currently available evidence from emergent high-resolution (0.1°) ocean model runs (Nooteboom et al., 2022) we consider "warm"-current invasion into the SW Pacific and AAG as the leading mechanism for forcing similar temperatures east and west of the TG. This however does not yet explain the extremely high temperatures in the high-latitude AAG or SW Pacific. Particularly the extremely high temperatures obtained from the various SST proxies remain difficult to approach in climate models that, for other regions and for regional MAAT proxies, produce satisfactory results.

5. Conclusions

The southwest Pacific Ocean (~50–60°S paleolatitude) was anomalously warm through much of the early Paleogene, and proxy-derived SSTs exceed modeled SST by ~10°C. Our data extend the area with extremely high proxy temperatures westward into the AAG, with broad implications for reconstruction of meridional temperature gradients and polar amplification that would be based on zonally averaged temperature or temperature patterns and general ocean circulation.

The new multi-proxy temperature records from the AAG reveal a subtle long-term or step-wise Late Paleocene warming on land and in the ocean, and, superimposed, two Late Paleocene transient "precursor" warming events, some ~300–400 and ~100 kyr prior to the PETM. The origin, geographical extent and magnitude of these transient events remain uncertain, but the existence of such relatively pronounced (regional) variability is remarkable.

The new data also emphasizes the persistence of high, but similar absolute temperatures and temperature evolution on both sides of a likely closed TG through the warmest periods of the Paleogene (late Paleocene, PETM and EECO). A strong influence of low-latitude ocean currents on both sides of the TG is not expected based on marine microfossil distributions or low-resolution models, yet should not be discarded as a mechanism that contributed to excessive regional warmth and particularly similar temperatures east and west of the TG.

A scenario with (seasonal) low-latitude influences on both sides of the TG may become a preferred scenario when high-resolution, eddy-resolving, modeling can be shown to accurately represent surface water conditions in the Paleocene-Eocene Southern Ocean. Moreover, the difference between low and high-resolution climate model runs may shed some light on SST over- or underestimates east and west of the TG. In addition, a more accurate representation of seasonality in the coastal-marginal marine settings may aid in resolving the influence of proxy biases.

However, even if part of the model-data discrepancy can be resolved by higher-resolution climate modeling, including an accurate representation of paleogeography, it is likely other challenges, such as the offset between

SST and MAAT estimates, still limit our understanding of these distinctly non-analog climates as they prevailed in the southern mid to high-latitudes. Some of these directly complicate comparison of proxy data to climate models, such as the influence of paleogeographic and paleobathymetric boundary conditions; factors that are both difficult to reconstruct and to accurately represent in models.

Conflict of Interest

The authors declare no conflicts of interest relevant to this study.

Data Availability Statement

All newly generated data are available via the Pangaea database (Frieling et al., 2022). Requests for raw materials should be directed to P.K. Bijl (p.k.bijl@uu.nl).

Acknowledgments

We thank G. Dammers, E.P. Huurdeman, K. Nierop, C. Rem, and A. van Leeuwen for assistance in palynological processing and organic geochemical analyses. E. Hopmans is thanked for assistance and discussions on UHPLC-MS data. E.P. Huurdeman is acknowledged for work on the Latrobe-1 core as part of a Master's thesis. SJG was supported by the Australian Integrated Ocean Drilling Program office. JP acknowledges support by the German Research Foundation (DFG; Grant PR 651/24-1). AS thanks the European Research Council for consolidator Grant 771497. PKB acknowledges support from NWO Vernieuwingsimpuls Veni Grant 863.13.002. We are thankful for constructive reviews, suggestions and comments from the associate editor, an anonymous reviewer and Kate Littler that helped improve this manuscript. References used in Supporting information files: (De Jonge, Hopmans, et al., 2014; Frieling et al., 2018; Huurdeman et al., 2021; Kim et al., 2010; Naafs, Inglis, et al., 2017; Naafs, McCormick, et al., 2018; Sluijs et al., 2011, 2020; Tierney & Tingley, 2015; Zonneveld et al., 2008, 2019).

References

Antoine, D., Andrt, J. M., & Morel, A. (1996). Oceanic primary production: 2. Estimation at global scale from satellite (Coastal Zone Color Scanner) chlorophyll. *Global Biogeochemical Cycles*, *10*(1), 57–69. https://doi.org/10.1029/95GB02832

Arditto, P. A. (1995). The eastern Otway Basin Wangerrip Group revisited using an integrated sequence methodology. *The APEA Journal*, *35*, 372–384.

Armstrong McKay, D. I., & Lenton, T. M. (2018). Reduced carbon cycle resilience across the Palaeocene–Eocene Thermal Maximum. *Climate of the Past*, *14*(10), 1515–1527. https://doi.org/10.5194/cp-14-1515-2018

Baatsen, M., von der Heydt, A. S., Huber, M., Kliphuis, M. A., Bijl, P. K., Sluijs, A., & Dijkstra, H. A. (2018). Equilibrium state and sensitivity of the simulated middle-to-late Eocene climate. *Climate of the Past Discussions*, 1–49. https://doi.org/10.5194/cp-2018-43

Baatsen, M., Von Der Heydt, A. S., Huber, M., Kliphuis, M. A., Bijl, P. K., Sluijs, A., & Dijkstra, H. A. (2020). The middle to late Eocene greenhouse climate modelled using the CESM 1.0.5. *Climate of the Past*, *16*(6), 2573–2597. https://doi.org/10.5194/cp-16-2573-2020

Babila, T. L., Penman, D. E., Standish, C. D., Doubrawa, M., Bralower, T. J., Robinson, M. M., et al. (2022). Surface ocean warming and acidification driven by rapid carbon release precedes. *Paleocene-Eocene Thermal Maximum*, *1025*, 1–14.

Bale, N. J., Palatinszky, M., Rijpstra, W. I. C., Herbold, C. W., Wagner, M., & Damsté, J. S. S. (2019). Membrane lipid composition of the moderately thermophilic ammonia-oxidizing archaeon "Candidatus Nitrosotenuis uzonensis" at different growth temperatures. *Applied and Environmental Microbiology*, *85*(20). https://doi.org/10.1128/AEM.01332-19

Baxter, A. J., Hopmans, E. C., Russell, J. M., Sinninghe, J. S., Sinninghe Damsté, J. S., & Sinninghe, J. S. (2019). Bacterial GMGTs in East African lake sediments: Their potential as palaeotemperature indicators. *Geochimica et Cosmochimica Acta*, *259*, 155–169. https://doi.org/10.1016/j.gca.2019.05.039

Baxter, A. J., van Bree, L. G. J., Peterse, F., Hopmans, E. C., Villanueva, L., Verschuren, D., & Sinninghe Damsté, J. S. (2021). Seasonal and multi-annual variation in the abundance of isoprenoid GDGT membrane lipids and their producers in the water column of a meromictic equatorial crater lake (Lake Chala, East Africa). *Quaternary Science Reviews*, *273*, 107263. https://doi.org/10.1016/j.quascirev.2021.107263

Bijl, P. K., Bendle, J. A. P., Bohaty, S. M., Pross, J., Schouten, S., Tauxe, L., et al. (2013). Eocene cooling linked to early flow across the Tasmanian Gateway. *Proceedings of the National Academy of Sciences of the United States of America*, *110*(24), 9645–9650. https://doi.org/10.1073/pnas.1220872110

Bijl, P. K., Brinkhuis, H., Egger, L. M., Eldrett, J. S., Frieling, J., Grothe, A., et al. (2016). Comment on 'Wetzeliella and its allies—The "hole" story: A taxonomic revision of the Paleogene dinoflagellate subfamily Wetzelielloideae' by Williams et al. (2015). *Palynology*, *6122*(3), 1–7. https://doi.org/10.1080/01916122.2016.1235056

Bijl, P. K., Frieling, J., Cramwinckel, M. J., Boschman, C., Sluijs, A., & Peterse, F. (2021). Maastrichtian–Rupelian paleoclimates in the southwest Pacific—A critical re-evaluation of biomarker paleothermometry and dinoflagellate cyst paleoecology at Ocean Drilling Program Site 1172. *Climate of the Past*, *17*(6), 2393–2425. https://doi.org/10.5194/cp-17-2393-2021

Bijl, P. K., Pross, J., Warnaar, J., Stickley, C. E., Huber, M., Guerstein, R., et al. (2011). Environmental forcings of Paleogene Southern Ocean dinoflagellate biogeography. *Paleoceanography*, *26*(1), 1–12. https://doi.org/10.1029/2009PA001905

Bijl, P. K., Schouten, S., Sluijs, A., Reichart, G.-J., Zachos, J. C., & Brinkhuis, H. (2009). Early Palaeogene temperature evolution of the southwest Pacific Ocean. *Nature*, *461*(7265), 776–779. https://doi.org/10.1038/nature08399

Bijl, P. K., Sluijs, A., & Brinkhuis, H. (2013). A magneto- and chemostratigraphically calibrated dinoflagellate cyst zonation of the early Palaeogene South Pacific Ocean. *Earth-Science Reviews*, *124*(0), 1–31. https://doi.org/10.1016/j.earscirev.2013.04.010

Bowen, G. J., Maibauer, B. J., Kraus, M. J., Röhl, U., Westerhold, T., Steimke, A., et al. (2015). Two massive, rapid releases of carbon during the onset of the Palaeocene-Eocene thermal maximum. *Nature Geoscience*, *8*(1), 44–47. https://doi.org/10.1038/ngeo2316

Burke, K. D., Williams, J. W., Chandler, M. A., Haywood, A. M., Lunt, D. J., & Otto-Bliesner, B. L. (2018). Pliocene and Eocene provide best analogs for near-future climates. *Proceedings of the National Academy of Sciences of the United States of America*, *115*(52), 201809600. https://doi.org/10.1073/pnas.1809600115

Cande, S. C., & Stock, J. M. (2004). Cenozoic reconstructions of the Australia-New Zealand-South Pacific sector of Antarctica. *Geophysical Monograph Series*, *151*, 5–17. https://doi.org/10.1029/151GM02

Carpenter, R. J., Jordan, G. J., Macphail, M. K., & Hill, R. S. (2012). Near-tropical early Eocene terrestrial temperatures at the Australo-Antarctic margin, western Tasmania. *Geology*, *40*(3), 267–270. https://doi.org/10.1130/G32584.1

Contreras, L., Pross, J., Bijl, P. K., Koutsodendris, A., Raine, J. I., van de Schootbrugge, B., & Brinkhuis, H. (2013). Early to middle Eocene vegetation dynamics at the Wilkes Land Margin (Antarctica). *Review of Palaeobotany and Palynology*, *197*, 119–142. https://doi.org/10.1016/j.revpalbo.2013.05.009

Contreras, L., Pross, J., Bijl, P. K., O'Hara, R. B., Raine, J. I., Sluijs, A., & Brinkhuis, H. (2014). Southern high-latitude terrestrial climate change during the Palaeocene–Eocene derived from a marine pollen record (ODP Site 1172, East Tasman Plateau). *Climate of the Past*, *10*(4), 1401–1420. https://doi.org/10.5194/cp-10-1401-2014

Coxall, H. K., Huck, C. E., Huber, M., Lear, C. H., Legarda-Lisarri, A., O'Regan, M., et al. (2018). Export of nutrient rich Northern Component Water preceded early Oligocene Antarctic glaciation/704/106/413/704/829/704/106/2738 article. *Nature Geoscience*, *11*(3), 190–196. https://doi.org/10.1038/s41561-018-0069-9

Cramer, B. S., Wright, J. D., Kent, D. V., & Aubry, M.-P. (2003). Orbital climate forcing of d^{13}C excursions in the late Paleocene-early Eocene (chrons C24n-C25n). *Paleoceanography*, *18*(4), 21. Retrieved from http://www.scopus.com/inward/record.url?eid=2-s2.0-1642357632&partnerID=40&md5=e225c616d2870c017d457b320c7144a2

Cramwinckel, M. J., Huber, M., Kocken, I. J., Agnini, C., Bijl, P. K., Bohaty, S. M., et al. (2018). Synchronous tropical and polar temperature evolution in the Eocene. *Nature*, *559*(7714), 382–386. https://doi.org/10.1038/s41586-018-0272-2

Cramwinckel, M. J., van der Ploeg, R., van Helmond, N. A. G. M., Waarlo, N., Agnini, C., Bijl, P. K., et al. (2022). Deoxygenation and organic carbon sequestration in the Tethyan realm associated with the middle Eocene climatic optimum. *GSA Bulletin*, 1–17. https://doi.org/10.1130/b36280.1

Cramwinckel, M. J., Woelders, L., Huurdeman, E. P., Peterse, F., Gallagher, S. J., Pross, J., et al. (2020). Surface-circulation change in the southwest Pacific Ocean across the middle Eocene climatic optimum: Inferences from dinoflagellate cysts and biomarker paleothermometry. *Climate of the Past*, *16*(5), 1667–1689. https://doi.org/10.5194/cp-16-1667-2020

Crouch, E. M., Willumsen, P. S., Kulhanek, D. K., & Gibbs, S. J. (2014). A revised Paleocene (Teurian) dinoflagellate cyst zonation from eastern New Zealand. *Review of Palaeobotany and Palynology*, *202*, 47–79. https://doi.org/10.1016/j.revpalbo.2013.12.004

De La Torre, J. R., Walker, C. B., Ingalls, A. E., Könneke, M., & Stahl, D. A. (2008). Cultivation of a thermophilic ammonia oxidizing archaeon synthesizing crenarchaeol. *Environmental Microbiology*, *10*(3), 810–818. https://doi.org/10.1111/j.1462-2920.2007.01506.x

Dearing Crampton-Flood, E., van der Weijst, C. M. H., van der Molen, G., Bouquet, M., Yedema, Y., Donders, T. H., et al. (2021). Identifying marine and freshwater overprints on soil-derived branched GDGT temperature signals in Pliocene Mississippi and Amazon River fan sediments. *Organic Geochemistry*, *154*, 104200. https://doi.org/10.1016/j.orggeochem.2021.104200

De Jonge, C., Hopmans, E. C., Zell, C. I., Kim, J.-H., Schouten, S., & Sinninghe Damsté, J. S. (2014). Occurrence and abundance of 6-methyl branched glycerol dialkyl glycerol tetraethers in soils: Implications for palaeoclimate reconstruction. *Geochimica et Cosmochimica Acta*, *141*, 97–112. https://doi.org/10.1016/j.gca.2014.06.013

De Jonge, C., Stadnitskaia, A., Hopmans, E. C., Cherkashov, G., Fedotov, A., & Sinninghe Damsté, J. S. (2014). In situ produced branched glycerol dialkyl glycerol tetraethers in suspended particulate matter from the Yenisei River, Eastern Siberia. *Geochimica et Cosmochimica Acta*, *125*, 476–491. https://doi.org/10.1016/j.gca.2013.10.031

Dickens, G. R., O'Neil, J. R., Rea, D. K., & Owen, R. M. (1995). Dissociation of oceanic methane hydrate as a cause of the carbon isotope excursion at the end of the Paleocene. *Paleoceanography*, *10*(6), 965–971. https://doi.org/10.1029/95PA02087

Douglas, P. M. J., Affek, H. P., Ivany, L. C., Houben, A. J. P., Sijp, W. P., Sluijs, A., et al. (2014). Pronounced zonal heterogeneity in Eocene southern high-latitude sea surface temperatures. *Proceedings of the National Academy of Sciences of the United States of America*, *111*(18), 1–6. https://doi.org/10.1073/pnas.1321441111

Dunkley Jones, T., Lunt, D. J., Schmidt, D. N., Ridgwell, A. J., Sluijs, A., Valdes, P. J., & Maslin, M. A. (2013). Climate model and proxy data constraints on ocean warming across the Paleocene–Eocene Thermal Maximum. *Earth-Science Reviews*, *125*(0), 123–145. https://doi.org/10.1016/j.earscirev.2013.07.004

Evans, D., Sagoo, N., Renema, W., Cotton, L. J., Müller, W., Todd, J. A., et al. (2018). Eocene greenhouse climate revealed by coupled clumped Isotope-Mg/Ca thermometry. *Proceedings of the National Academy of Sciences of the United States of America*, *115*(6), 1174–1179. https://doi.org/10.1073/pnas.1714744115

Frieling, J., Bohaty, S. M., Cramwinckel, M. J., Gallagher, S. J., Holdgate, G. R., Reichgelt, T., et al. (2022). Temperature proxy data for the late Paleocene and Paleocene-Eocene Thermal Maximum from the Australo-Antarctic Gulf [Dataset]. Pangaea. https://doi.org/10.1594/PANGAEA.949912

Frieling, J., Gebhardt, H., Huber, M., Adekeye, O. A., Akande, S. O., Reichart, G.-J., et al. (2017). Extreme warmth and heat-stressed plankton in the tropics during the Paleocene-Eocene Thermal Maximum. *Science Advances*, *3*(3), e1600891. https://doi.org/10.1126/sciadv.1600891

Frieling, J., Huurdeman, E. P., Rem, C. C. M., Donders, T. H., Pross, J., Bohaty, S. M., et al. (2018). Identification of the Paleocene–Eocene boundary in coastal strata in the Otway Basin, Victoria, Australia. *Journal of Micropalaeontology*, *37*(1), 317–339. https://doi.org/10.5194/jm-37-317-2018

Frieling, J., Peterse, F., Lunt, D. J. J., Bohaty, S. M. M., Damsté, J. S. S., Reichart, G.-J.-J., & Sluijs, A. (2019). Widespread warming before and elevated barium burial during the Paleocene-Eocene Thermal Maximum: Evidence for methane hydrate release? *Paleoceanography and Paleoclimatology*, *34*(4), 2018PA003425. https://doi.org/10.1029/2018PA003425

Frieling, J., & Sluijs, A. (2018). Towards quantitative environmental reconstructions from ancient non-analogue microfossil assemblages: Ecological preferences of Paleocene—Eocene dinoflagellates. *Earth-Science Reviews*, *185*, 956–973. https://doi.org/10.1016/j.earscirev.2018.08.014

Gouretski, V. V., & Koltermann, K. P. (2004). WOCE global hydrographic climatology. *Berichte Des Bundesamtes Fur Seeschifffahrt Und Hydrographie*. https://doi.org/10.5065/GS51-V170

Greenwood, D. R., Moss, P. T., Rowett, A. I., Vadala, A. J., & Keefe, R. L. (2003). Plant communities and climate change in southeastern Australia during the early Paleogene. In *Special Paper 369: Causes and consequences of globally warm climates in the early Paleogene* (pp. 365–380). Geological Society of America. https://doi.org/10.1130/0-8137-2369-8.365

Hernández-Sánchez, M. T., Woodward, E. M. S., Taylor, K. W. R., Henderson, G. M., & Pancost, R. D. (2014). Variations in GDGT distributions through the water column in the south east Atlantic Ocean. *Geochimica et Cosmochimica Acta*, *132*, 337–348. https://doi.org/10.1016/j.gca.2014.02.009

Hines, B. R., Hollis, C. J., Atkins, C. B., Baker, J. A., Morgans, H. E. G., & Strong, P. C. (2017). Reduction of oceanic temperature gradients in the early Eocene Southwest Pacific Ocean. *Palaeogeography, Palaeoclimatology, Palaeoecology*, *475*, 41–54. https://doi.org/10.1016/j.palaeo.2017.02.037

Hirahara, S., Ishii, M., & Fukuda, Y. (2014). Centennial-scale sea surface temperature analysis and its uncertainty. *Journal of Climate*, *27*(1), 57–75. https://doi.org/10.1175/JCLI-D-12-00837.1

Hollis, C. J., Dunkley Jones, T., Anagnostou, E., Bijl, P. K., Cramwinckel, M. J., Cui, Y., et al. (2019). The DeepMIP contribution to PMIP4: Methodologies for selection, compilation and analysis of latest Paleocene and early Eocene climate proxy data, incorporating version 0.1 of the DeepMIP database. *Geoscientific Model Development*, *12*(7), 3149–3206. https://doi.org/10.5194/gmd-12-3149-2019

Hollis, C. J., Handley, L., Crouch, E. M., Morgans, H. E. G., Baker, J. A., Creech, J., et al. (2009). Tropical sea temperatures in the high-latitude South Pacific during the Eocene. *Geology*, *37*(2), 99–102. https://doi.org/10.1130/G25200A.1

Hollis, C. J., Hines, B. R., Littler, K., Villasante-Marcos, V., Kulhanek, D. K., Strong, C. P., et al. (2015). The Paleocene–Eocene Thermal Maximum at DSDP Site 277, Campbell Plateau, southern Pacific Ocean. *Climate of the Past*, *11*(7), 1009–1025. https://doi.org/10.5194/cp-11-1009-2015

Hollis, C. J., Taylor, K. W. R., Handley, L., Pancost, R. D., Huber, M., Creech, J. B., et al. (2012). Early Paleogene temperature history of the southwest Pacific Ocean: Reconciling proxies and models. *Earth and Planetary Science Letters*, *349*(350), 53–66. https://doi.org/10.1016/j.epsl.2012.06.024

Hopmans, E. C., Schouten, S., & Sinninghe Damsté, J. S. (2016). The effect of improved chromatography on GDGT-based palaeoproxies. *Organic Geochemistry*, *93*, 1–6. https://doi.org/10.1016/j.orggeochem.2015.12.006

Hopmans, E. C., Weijers, J. W. H., Schefuß, E., Herfort, L., Sinninghe Damsté, J. S., & Schouten, S. (2004). A novel proxy for terrestrial organic matter in sediments based on branched and isoprenoid tetraether lipids. *Earth and Planetary Science Letters*, *224*(1–2), 107–116. https://doi.org/10.1016/j.epsl.2004.05.012

Huber, M., Brinkhuis, H., Stickley, C. E., Döös, K., Sluijs, A., Warnaar, J., et al. (2004). Eocene circulation of the Southern Ocean: Was Antarctica kept warm by subtropical waters? *Paleoceanography*, *19*(4). https://doi.org/10.1029/2004PA001014

Huck, C. E., van de Flierdt, T., Bohaty, S. M., & Hammond, S. J. (2017). Antarctic climate, Southern Ocean circulation patterns, and deep water formation during the Eocene. *Paleoceanography*, *32*(7), 674–691. https://doi.org/10.1002/2017PA003135

Hurley, S. J., Elling, F. J., Könneke, M., Buchwald, C., Wankel, S. D., Santoro, A. E., et al. (2016). Influence of ammonia oxidation rate on thaumarchaeal lipid composition and the TEX86 temperature proxy. *Proceedings of the National Academy of Sciences of the United States of America*, *113*(28), 7762–7767. https://doi.org/10.1073/pnas.1518534113

Hurley, S. J., Lipp, J. S., Close, H. G., Hinrichs, K. U., & Pearson, A. (2018). Distribution and export of isoprenoid tetraether lipids in suspended particulate matter from the water column of the western Atlantic Ocean. *Organic Geochemistry*, *116*, 90–102. https://doi.org/10.1016/j.orggeochem.2017.11.010

Huurdeman, E. P., Frieling, J., Reichgelt, T., Bijl, P. K., Bohaty, S. M., Holdgate, G. R., et al. (2021). Rapid expansion of meso-megathermal rain forests into the southern high latitudes at the onset of the Paleocene-Eocene Thermal Maximum. *Geology*, *49*(1), 40–44. https://doi.org/10.1130/G47343.1

Inglis, G. N., Farnsworth, A., Collinson, M. E., Carmichael, M. J., Naafs, B. D. A., Lunt, D. J., et al. (2019). Terrestrial environmental change across the onset of the PETM and the associated impact on biomarker proxies: A cautionary tale. *Global and Planetary Change*, *181*, 102991. https://doi.org/10.1016/j.gloplacha.2019.102991

Inglis, G. N., Farnsworth, A., Lunt, D. J., Foster, G. L., Hollis, C. J., Pagani, M., et al. (2015). Descent towards the Icehouse: Eocene sea surface cooling inferred from GDGT distributions. *Paleoceanography*, *30*(7), 1000–1020. https://doi.org/10.1002/2014PA002723

John, C. M., Banerjee, N. R., Longstaffe, F. J., Sica, C., Law, K. R., & Zachos, J. C. (2012). Clay assemblage and oxygen isotopic constraints on the weathering response to the Paleocene-Eocene Thermal Maximum, east coast of North America. *Geology*, *40*(7), 591–594. https://doi.org/10.1130/G32785.1

Judd, E. J., Bhattacharya, T., & Ivany, L. C. (2020). A dynamical framework for interpreting Ancient sea surface temperatures. *Geophysical Research Letters*, *47*(15), e2020GL089044. https://doi.org/10.1029/2020GL089044

Kim, J. H., Schouten, S., Rodrigo-Gámiz, M., Rampen, S., Marino, G., Huguet, C., et al. (2015). Influence of deep-water derived isoprenoid tetraether lipids on the TEX86H paleothermometer in the Mediterranean Sea. *Geochimica et Cosmochimica Acta*, *150*, 125–141. https://doi.org/10.1016/j.gca.2014.11.017

Kim, J. H., van der Meer, J., Schouten, S., Helmke, P., Willmott, V., Sangiorgi, F., et al. (2010). New indices and calibrations derived from the distribution of crenarchaeal isoprenoid tetraether lipids: Implications for past sea surface temperature reconstructions. *Geochimica et Cosmochimica Acta*, *74*(16), 4639–4654. https://doi.org/10.1016/j.gca.2010.05.027

Kirkels, F. M. S. A., Usman, M. O., & Peterse, F. (2022). Distinct sources of bacterial branched GMGTs in the Godavari River basin (India) and Bay of Bengal sediments. *Organic Geochemistry*, *167*, 104405. https://doi.org/10.1016/j.orggeochem.2022.104405

Lagabrielle, Y., Goddéris, Y., Donnadieu, Y., Malavieille, J., & Suarez, M. (2009). The tectonic history of Drake Passage and its possible impacts on global climate. *Earth and Planetary Science Letters*, *279*(3–4), 197–211. https://doi.org/10.1016/j.epsl.2008.12.037

Lauretano, V., Littler, K., Polling, M., Zachos, J. C., & Lourens, L. J. (2015). Frequency, magnitude and character of hyperthermal events at the onset of the Early Eocene Climatic Optimum. *Climate of the Past*, *11*(10), 1313–1324. https://doi.org/10.5194/cp-11-1313-2015

Liu, X. L., Summons, R. E., & Hinrichs, K. U. (2012). Extending the known range of glycerol ether lipids in the environment: Structural assignments based on tandem mass spectral fragmentation patterns. *Rapid Communications in Mass Spectrometry*, *26*(19), 2295–2302. https://doi.org/10.1002/rcm.6355

Lunt, D. J., Bragg, F., Chan, W.-L., Hutchinson, D. K., Ladant, J.-B., Morozova, P., et al. (2021). DeepMIP: Model intercomparison of early Eocene climatic optimum (EECO) large-scale climate features and comparison with proxy data. *Climate of the Past*, *17*(1), 203–227. https://doi.org/10.5194/cp-17-203-2021

Lunt, D. J., Farnsworth, A., Loptson, C., FosterMarkwick, G. P., Markwick, P., O'Brien, C. L., et al. (2016). Palaeogeographic controls on climate and proxy interpretation. *Climate of the Past*, *12*(5), 1181–1198. https://doi.org/10.5194/cp-12-1181-2016

Lunt, D. J., Huber, M., Anagnostou, E., Baatsen, M. L. J., Caballero, R., DeConto, R., et al. (2017). The DeepMIP contribution to PMIP4: Experimental design for model simulations of the EECO, PETM, and pre-PETM (version 1.0). *Geoscientific Model Development*, *10*(2), 889–901. https://doi.org/10.5194/gmd-10-889-2017

McInerney, F. A., & Wing, S. L. (2011). The Paleocene-Eocene thermal maximum: A perturbation of carbon cycle, climate, and biosphere with implications for the future. *Annual Review of Earth and Planetary Sciences*, *39*(1), 489–516. https://doi.org/10.1146/annurev-earth-040610-133431

Morii, H., Eguchi, T., Nishihara, M., Kakinuma, K., König, H., & Koga, Y. (1998). A novel ether core lipid with H-shaped C80-isoprenoid hydrocarbon chain from the hyperthermophilic methanogen methanothermus fervidus. *Biochimica et Biophysica Acta (BBA)—Lipids and Lipid Metabolism*, *1390*(3), 339–345. https://doi.org/10.1016/S0005-2760(97)00183-5

Müller, R. D., Zahirovic, S., Williams, S. E., Cannon, J., Seton, M., Bower, D. J., et al. (2019). A global plate model including lithospheric deformation along major rifts and orogens since the triassic. *Tectonics*, *38*(6), 1884–1907. https://doi.org/10.1029/2018TC005462

Naafs, B. D. A., Gallego-Sala, A. V., Inglis, G. N., & Pancost, R. D. (2017). Refining the global branched glycerol dialkyl glycerol tetraether (brGDGT) soil temperature calibration. *Organic Geochemistry*, *106*, 48–56. https://doi.org/10.1016/j.orggeochem.2017.01.009

Naafs, B. D. A., Inglis, G. N., Zheng, Y., Amesbury, M. J., Biester, H., Bindler, R., et al. (2017). Introducing global peat-specific temperature and pH calibrations based on brGDGT bacterial lipids. *Geochimica et Cosmochimica Acta*, *208*, 285–301. https://doi.org/10.1016/j.gca.2017.01.038

Naafs, B. D. A., McCormick, D., Inglis, G. N., & Pancost, R. D. (2018). Archaeal and bacterial H-GDGTs are abundant in peat and their relative abundance is positively correlated with temperature. *Geochimica et Cosmochimica Acta*, *227*, 156–170. https://doi.org/10.1016/j.gca.2018.02.025

Naafs, B. D. A., Rohrssen, M., Inglis, G. N., Lähteenoja, O., Feakins, S. J., Collinson, M. E., et al. (2018). High temperatures in the terrestrial mid-latitudes during the early Palaeogene. *Nature Geoscience*, *11*(10), 766–771. https://doi.org/10.1038/s41561-018-0199-0

Nooteboom, P. D., Baatsen, M., Bijl, P. K., Kliphuis, M. A., van Sebille, E., Sluijs, A., et al. (2022). Improved model-data agreement with strongly eddying ocean simulations in the middle-late Eocene. *Paleoceanography and Paleoclimatology*, *37*(8), 1–23. https://doi.org/10.1029/2021PA004405

Nooteboom, P. D., Delandmeter, P., van Sebille, E., Bijl, P. K., Dijkstra, H. A., & von der Heydt, A. S. (2020). Resolution dependency of sinking Lagrangian particles in ocean general circulation models. *PLoS One*, *15*, 1–16. https://doi.org/10.1371/journal.pone.0238650

O'Brien, C. L., Robinson, S. A., Pancost, R. D., Sinninghe Damsté, J. S., Schouten, S., Lunt, D. J., et al. (2017). Cretaceous sea-surface temperature evolution: Constraints from TEX 86 and planktonic foraminiferal oxygen isotopes. *Earth-Science Reviews*, *172*, 224–247. https://doi.org/10.1016/j.earscirev.2017.07.012

Pak, D. K., & Miller, K. G. (1992). Paleocene to Eocene benthic foraminiferal isotopes and assemblages: Implications for deepwater circulation. *Paleoceanography*, *7*(4), 405–422. https://doi.org/10.1029/92pa01234

Pancost, R. D., Taylor, K. W. R., Inglis, G. N., Kennedy, E. M., Handley, L., Hollis, C. J., et al. (2013). Early Paleogene evolution of terrestrial climate in the SW Pacific, southern New Zealand. *Geochemistry, Geophysics, Geosystems*, *14*(12), 5413–5429. https://doi.org/10.1002/2013GC004935

Pitcher, A., Villanueva, L., Hopmans, E. C., Schouten, S., Reichart, G. J., & Sinninghe Damsté, J. S. (2011). Niche segregation of ammonia-oxidizing archaea and anammox bacteria in the Arabian Sea oxygen minimum zone. *The ISME Journal*, *5*(12), 1896–1904. https://doi.org/10.1038/ismej.2011.60

Prebble, J. G., Crouch, E. M., Carter, L., Cortese, G., Bostock, H., & Neil, H. (2013). An expanded modern dinoflagellate cyst dataset for the southwest Pacific and southern hemisphere with environmental associations. *Marine Micropaleontology*, *101*, 33–48. https://doi.org/10.1016/j.marmicro.2013.04.004

Pross, J., Contreras, L., Bijl, P. K., Greenwood, D. R., Bohaty, S. M., Schouten, S., et al. (2012). Persistent near-tropical warmth on the Antarctic continent during the early Eocene epoch. *Nature*, *487*(7409), 73–77. https://doi.org/10.1038/nature11300

Reichgelt, T., Greenwood, D. R., Steinig, S., Conran, J. G., Hutchinson, D. K., Lunt, D. J., et al. (2022). Plant proxy evidence for high rainfall and productivity in the Eocene of Australia. *Paleoceanography and Paleoclimatology*, *37*, e2022PA004418. https://doi.org/10.1029/2022PA004418

Reichgelt, T., West, C. K., & Greenwood, D. R. (2018). The relation between global palm distribution and climate. *Scientific Reports*, *8*(1), 4721. https://doi.org/10.1038/s41598-018-23147-2

Sauermilch, I., Whittaker, J. M., Bijl, P. K., Totterdell, J. M., & Jokat, W. (2019). Tectonic, oceanographic, and climatic controls on the cretaceous-Cenozoic sedimentary record of the Australian-Antarctic Basin. *Journal of Geophysical Research: Solid Earth*, *124*(8), 7699–7724. https://doi.org/10.1029/2018JB016683

Sauermilch, I., Whittaker, J. M., Klocker, A., Munday, D. R., Hochmuth, K., Bijl, P. K., & LaCasce, J. H. (2021). Gateway-driven weakening of ocean gyres leads to Southern Ocean cooling. *Nature Communications*, *12*(1), 1–8. https://doi.org/10.1038/s41467-021-26658-1

Schneider-Mor, A., & Bowen, G. J. (2013). Coupled and decoupled responses of continental and marine organic-sedimentary systems through the Paleocene-Eocene thermal maximum, New Jersey margin, USA. *Paleoceanography*, *28*(1), 105–115. https://doi.org/10.1002/palo.20016

Schouten, S., Baas, M., Hopmans, E. C., Reysenbach, A. L., & Damsté, J. S. S. (2008). Tetraether membrane lipids of Candidatus "Aciduliprofundum boonei", a cultivated obligate thermoacidophilic euryarchaeote from deep-sea hydrothermal vents. *Extremophiles*, *12*(1), 119–124. https://doi.org/10.1007/s00792-007-0111-0

Schouten, S., Hopmans, E. C., Schefuß, E., & Sinninghe Damsté, J. S. (2002). Distributional variations in marine crenarchaeotal membrane lipids: A new tool for reconstructing ancient sea water temperatures? *Earth and Planetary Science Letters*, *204*(1–2), 265–274. https://doi.org/10.1016/S0012-821X(02)00979-2

Schouten, S., Hopmans, E. C., & Sinninghe Damsté, J. S. (2013). The organic geochemistry of glycerol dialkyl glycerol tetraether lipids: A review. *Organic Geochemistry*, *54*(0), 19–61. https://doi.org/10.1016/j.orggeochem.2012.09.006

Secord, R., Gingerich, P. D., Lohmann, K. C., & MacLeod, K. G. (2010). Continental warming preceding the Palaeocene-Eocene thermal maximum. *Nature*, *467*(7318), 955–958. https://doi.org/10.1038/nature09441

Seton, M., Müller, R. D., Zahirovic, S., Gaina, C., Torsvik, T. H., Shephard, G., et al. (2012). Global continental and ocean basin reconstructions since 200Ma. *Earth-Science Reviews*, *113*(3), 212–270. https://doi.org/10.1016/j.earscirev.2012.03.002

Sijp, W. P., England, M. H., & Huber, M. (2011). Effect of the deepening of the Tasman Gateway on the global ocean. *Paleoceanography*, *26*(4), 1–18. https://doi.org/10.1029/2011PA002143

Sijp, W. P., von der Heydt, A. S., & Bijl, P. K. (2016). Model simulations of early westward flow across the Tasman Gateway during the early Eocene. *Climate of the Past*, *12*(4), 807–817. https://doi.org/10.5194/cp-12-807-2016

Sijp, W. P., von der Heydt, A. S., Dijkstra, H. A., Flögel, S., Douglas, P. M. J. J., & Bijl, P. K. (2014). The role of ocean gateways on cooling climate on long time scales. *Global and Planetary Change*, *119*, 1–22. https://doi.org/10.1016/j.gloplacha.2014.04.004

Sinninghe Damsté, J. S. (2016). Spatial heterogeneity of sources of branched tetraethers in shelf systems: The geochemistry of tetraethers in the Berau River delta (Kalimantan, Indonesia). *Geochimica et Cosmochimica Acta*, *186*, 13–31. https://doi.org/10.1016/j.gca.2016.04.033

Sinninghe Damsté, J. S., Irene, C., Rijpstra, W., Hopmans, E. C., den Uijl, M. J., Weijers, J. W. H., & Schouten, S. (2018). The enigmatic structure of the crenarchaeol isomer. *Organic Geochemistry*, *124*, 22–28. https://doi.org/10.1016/j.orggeochem.2018.06.005

Sinninghe Damsté, J. S., Ossebaar, J., Schouten, S., & Verschuren, D. (2012). Distribution of tetraether lipids in the 25-ka sedimentary record of Lake Challa: Extracting reliable TEX 86 and MBT/CBT palaeotemperatures from an equatorial African lake. *Quaternary Science Reviews*, *50*, 43–54. https://doi.org/10.1016/j.quascirev.2012.07.001

Sinninghe Damsté, J. S., Schouten, S., Hopmans, E. C., Van Duin, A. C. T., & Geenevasen, J. A. J. (2002). Crenarchaeol: The characteristic core glycerol dibiphytanyl glycerol tetraether membrane lipid of cosmopolitan pelagic crenarchaeota. *Journal of Lipid Research*, *43*(10), 1641–1651. https://doi.org/10.1194/jlr.M200148-JLR200

Sluijs, A., Bijl, P. K., Schouten, S., Röhl, U., Reichart, G.-J., & Brinkhuis, H. (2011). Southern ocean warming, sea level and hydrological change during the Paleocene-Eocene thermal maximum. *Climate of the Past*, *7*(1), 47–61. https://doi.org/10.5194/cp-7-47-2011

Sluijs, A., Brinkhuis, H., Schouten, S., Bohaty, S. M., John, C. M., Zachos, J. C., et al. (2007). Environmental precursors to rapid light carbon injection at the Palaeocene/Eocene boundary. *Nature*, *450*(7173), 1218–1221. https://doi.org/10.1038/nature06400

Sluijs, A., & Dickens, G. R. (2012). Assessing offsets between the $\delta^{13}C$ of sedimentary components and the global exogenic carbon pool across early Paleogene carbon cycle perturbations. *Global Biogeochemical Cycles*, *26*(4), 1–14. https://doi.org/10.1029/2011GB004224

Sluijs, A., Frieling, J., Inglis, G. N., Nierop, K. G. J., Peterse, F., Sangiorgi, F., & Schouten, S. (2020). Late Paleocene–early Eocene Arctic Ocean sea surface temperatures: Reassessing biomarker paleothermometry at Lomonosov Ridge. *Climate of the Past*, *16*(6), 2381–2400. https://doi.org/10.5194/cp-16-2381-2020

Sutherland, R., Dickens, G. R., Blum, P., Agnini, C., Alegret, L., Asatryan, G., et al. (2019). Expedition 371 summary, *371*. https://doi.org/10.14379/iodp.proc.371.101.2019

Tang, X., Naafs, B. D. A., Pancost, R. D., Liu, Z., & Fan, T. (2021). Exploring the influences of temperature on "H-shaped" glycerol dialkyl glycerol tetraethers in a stratigraphic context: Evidence from two peat cores across the late. *Quaternary*, *8*, 1–7. https://doi.org/10.3389/feart.2020.541685

Taylor, K. W. R., Huber, M., Hollis, C. J., Hernandez-Sanchez, M. T., & Pancost, R. D. (2013). Re-evaluating modern and Palaeogene GDGT distributions: Implications for SST reconstructions. *Global and Planetary Change*, *108*, 158–174. https://doi.org/10.1016/j.gloplacha.2013.06.011

Thomas, D. J., Zachos, J. C., Bralower, T. J., Thomas, E., & Bohaty, S. M. (2002). Warming the fuel for the fire: Evidence for the thermal dissociation of methane hydrate during the Paleocene-Eocene Thermal Maximum dissociation of methane hydrate during the Paleocene-Eocene. *Geology*, *30*(12), 1067–1070. https://doi.org/10.1130/0091-7613(2002)030<1067:WTFFTF>2.0.CO;2

Tierney, J. E., & Tingley, M. P. (2015). A TEX86 surface sediment database and extended Bayesian calibration. *Scientific Data*, *2*(1), 150029. https://doi.org/10.1038/sdata.2015.29

Vahlenkamp, M., Niezgodzki, I., De Vleeschouwer, D., Lohmann, G., Bickert, T., & Pälike, H. (2018). Ocean and climate response to North Atlantic seaway changes at the onset of long-term Eocene cooling. *Earth and Planetary Science Letters*, *498*, 185–195. https://doi.org/10.1016/j.epsl.2018.06.031

van de Lagemaat, S. H. A., Swart, M. L. A., Vaes, B., Kosters, M. E., Boschman, L. M., Burton-Johnson, A., et al. (2021). Subduction initiation in the Scotia Sea region and opening of the Drake Passage: When and why? *Earth-Science Reviews*, *215*, 103551. https://doi.org/10.1016/j.earscirev.2021.103551

van Hinsbergen, D. J. J., de Groot, L. V., van Schaik, S. J., Spakman, W., Bijl, P. K., Sluijs, A., et al. (2015). A paleolatitude calculator for paleoclimate studies. *PLoS One*, *10*(6), e0126946. https://doi.org/10.1371/journal.pone.0126946

Weijers, J. W. H., Lim, K. L. H., Aquilina, A., Damsté, J. S. S., & Pancost, R. D. (2011). Biogeochemical controls on glycerol dialkyl glycerol tetraether lipid distributions in sediments characterized by diffusive methane flux. *Geochemistry, Geophysics, Geosystems*, *12*(10), Q10010. https://doi.org/10.1029/2011GC003724

Weijers, J. W. H., Schouten, S., Spaargaren, O. C., & Sinninghe Damsté, J. S. (2006). Occurrence and distribution of tetraether membrane lipids in soils: Implications for the use of the TEX86 proxy and the BIT index. *Organic Geochemistry*, *37*(12), 1680–1693. https://doi.org/10.1016/j.orggeochem.2006.07.018

Weijers, J. W. H., Schouten, S., van den Donker, J. C., Hopmans, E. C., & Sinninghe Damsté, J. S. (2007). Environmental controls on bacterial tetraether membrane lipid distribution in soils. *Geochimica et Cosmochimica Acta*, *71*(3), 703–713. https://doi.org/10.1016/j.gca.2006.10.003

Westerhold, T., Marwan, N., Drury, A. J., Liebrand, D., Agnini, C., Anagnostou, E., et al. (2020). An astronomically dated record of Earth's climate and its predictability over the last 66 million years. *Science*, *369*(6509), 1383–1388. https://doi.org/10.1126/SCIENCE.ABA6853

Westerhold, T., Röhl, U., Donner, B., & Zachos, J. C. (2018). Global extent of early Eocene hyperthermal events: A new Pacific benthic foraminiferal isotope record from Shatsky rise (ODP Site 1209). *Paleoceanography and Paleoclimatology*, *0*, 1–17. https://doi.org/10.1029/2017PA003306

Willard, D. A., Donders, T. H., Reichgelt, T., Greenwood, D. R., Sangiorgi, F., Peterse, F., et al. (2019). Arctic vegetation, temperature, and hydrology during Early Eocene transient global warming events. *Global and Planetary Change*, *178*, 139–152. https://doi.org/10.1016/j.gloplacha.2019.04.012

Williams, G. L., Fensome, R. A., & MacRae, R. A. (2017). The Lentin and Williams index of fossil dinoflagellates 2017 edition. In *American association of petroleum geologists contribution series* (Vol. 48).

Williams, S. E., Whittaker, J. M., Halpin, J. A., & Müller, R. D. (2019). Australian-Antarctic breakup and seafloor spreading: Balancing geological and geophysical constraints. *Earth-Science Reviews*, *188*, 41–58. https://doi.org/10.1016/j.earscirev.2018.10.011

Xie, S., Liu, X.-L., Schubotz, F., Wakeham, S. G., & Hinrichs, K.-U. (2014). Distribution of glycerol ether lipids in the oxygen minimum zone of the Eastern Tropical North Pacific Ocean. *Organic Geochemistry*, *71*, 60–71. https://doi.org/10.1016/j.orggeochem.2014.04.006

Zachos, J. C., Rohl, U., Schellenberg, S. A., Sluijs, A., Hodell, D. A., Kelly, D. C., et al. (2005). Rapid acidification of the ocean during the Paleocene-Eocene Thermal Maximum. *Science*, *308*(5728), 1611–1615. https://doi.org/10.1126/science.1109004

Zhang, Y. G., Pagani, M., & Wang, Z. (2016). Ring Index: A new strategy to evaluate the integrity of TEX 86 paleothermometry. *Paleoceanography*, *31*(2), 220–232. https://doi.org/10.1002/2015PA002848

Zhang, Y. G., Zhang, C. L., Liu, X. L., Li, L., Hinrichs, K. U., & Noakes, J. E. (2011). Methane Index: A tetraether archaeal lipid biomarker indicator for detecting the instability of marine gas hydrates. *Earth and Planetary Science Letters*, *307*(3–4), 525–534. https://doi.org/10.1016/j.epsl.2011.05.031

Zhu, J., Poulsen, C. J., & Tierney, J. E. (2019). Simulation of Eocene extreme warmth and high climate sensitivity through cloud feedbacks. *Science Advances*, *5*(9), eaax1874. https://doi.org/10.1126/sciadv.aax1874

Zonneveld, K. A. F., Gray, D. D., Kuhn, G., & Versteegh, G. J. M. (2019). Postdepositional aerobic and anaerobic particulate organic matter degradation succession reflected by dinoflagellate cysts: The Madeira Abyssal Plain revisited. *Marine Geology*, *408*, 87–109. https://doi.org/10.1016/j.margeo.2018.11.010

Zonneveld, K. A. F., Marret, F., Versteegh, G. J. M., Bogus, K., Bonnet, S., Bouimetarhan, I., et al. (2013). Atlas of modern dinoflagellate cyst distribution based on 2405 data points. *Review of Palaeobotany and Palynology*, *191*, 1–197. https://doi.org/10.1016/j.revpalbo.2012.08.003

Zonneveld, K. A. F., Versteegh, G. J. M., & Kodrans-Nsiah, M. (2008). Preservation and organic chemistry of late Cenozoic organic-walled dinoflagellate cysts: A review. *Marine Micropaleontology*, *68*(1), 179–197. https://doi.org/10.1016/j.marmicro.2008.01.015